Doctoral Dissertation

Studies on Poly(γ-glutamic acid)-based Hydrogels for Potential Biomedical Applications

(生物医学応用を指向したポリ（γ-グルタミン酸）ハイドロゲルに関する研究)

MENG WEI

June 2022

Graduate School of Engineering

Osaka University

Content

General Introduction

Responsive hydrogels

Smart/stimuli-responsive hydrogels are extraordinary three-dimensional (3D) scaffolds used in tissue engineering and other biomedical application. The volume or phase transition of responsive hydrogels can be varied under different physicochemical and biological stimulations (**Figure 1**).[1] Temperature and pH-responsive hydrogels are the most explored since they are highly adapted to physicochemical characteristics of human body. Based on the difference between body temperature (37°C) and room temperature, and the pH gradients in the gastrointestinal environment or between tumor and normal cells, responsive hydrogels are highly suitable for the application in tissue engineering and drug delivery.[2]

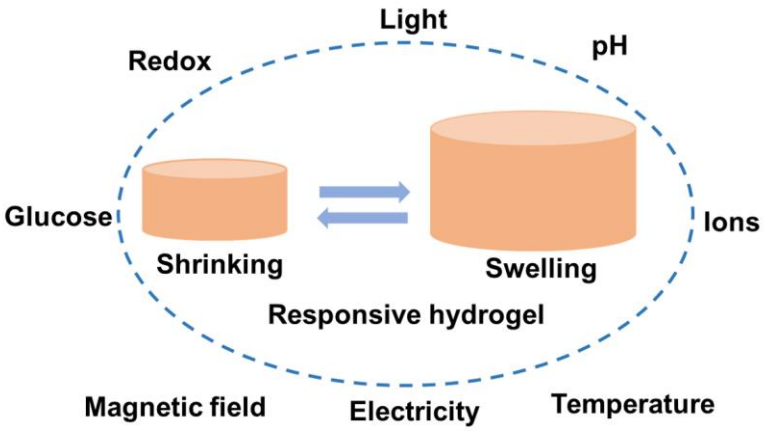

Figure 1. Stimulus-responsive hydrogels experience a dramatic volume/phase transition with reversible swelling/shrinking behaviors in response to a variety of environmental stimuli.

The injectability is beneficial for the practical application of responsive hydrogels employed as tissue engineering scaffolds and drug delivery. Recently, there has been a lot of interest in injectable hydrogels prepared by *in situ* chemical reactions or by the sol-gel phase transition. Before injection, these materials can easily flow as liquid, and when injected into the body they can be turned into hydrogel.[3] They provide the aqueous conditions for cell growth, support mechanical strength for cells, and use as delivery matrices for drug or bioactive molecules.[4] Thanks to the gel that forms after

injection, the injectable matrix can be implanted in the human body with minimally invasive surgeries, which reduces patient pain, and bioactive molecules or cells can be added successfully by mixing before injection.[5,6]

Enzymatic cross-linking is a green and facile method to fabricate injectable hydrogels owing to the tunable mechanical properties, efficient gelation process and physiological reaction conditions.[7] The hydrogels could be formed under the stimulation of horseradish peroxidase (HRP) and hydrogen peroxide (H_2O_2). HRP is a type of hemoprotein with a single chain that induces the conjugation of phenol and aniline compounds in the presence of H_2O_2. The mechanism of enzymatic cross-linking is described in **Figure 2a**. One H_2O_2 molecule is utilized by one HRP in a catalytic cycle in which two phenolic radicals are generated from two phenols, resulting in leave two water molecules. The crosslinking between the polymer-phenol compounds is established when the phenolic radicals are paired with each other. The *ortho*-carbon of the aromatic ring forms the more prevalent C-C coupling, while the *ortho*-carbon and phenolic oxygen produce C-O coupling (**Figure 2b**).[8,9] Based on the catalytic mechanism, the gelation rate and stiffness of hydrogels could be adjusted easily. The drug delivery in pharmaceutics or cell-growing depots for tissue regeneration can be achieved by HRP-mediated enzymatic cross-linking system.[10,11]

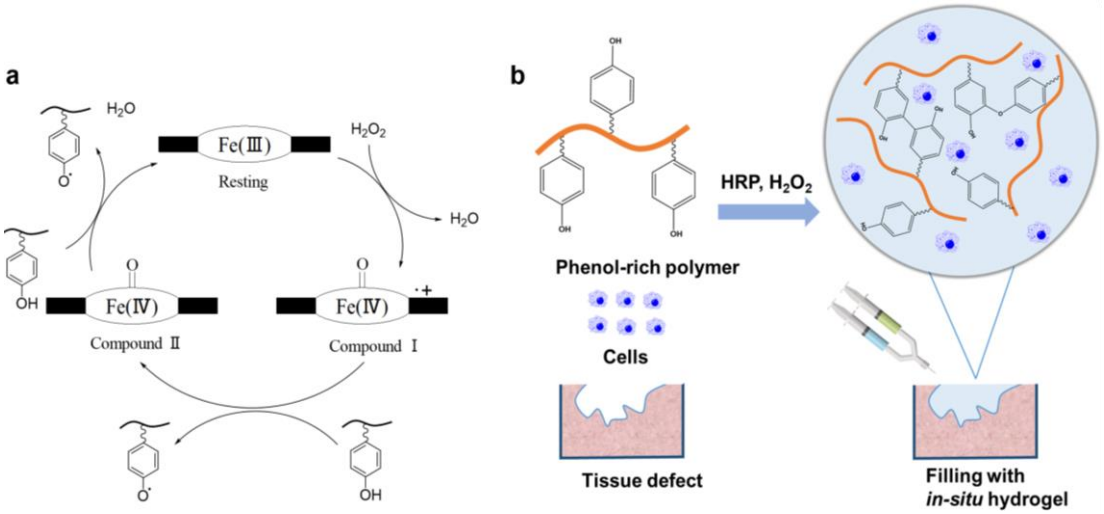

Figure 2. (a) The mechanism of enzymatic cross-linking. (b) The preparation of hydrogel *via* enzymatic cross-linking.

Responsive hydrogels for tissue engineering scaffolds

Native tissues regulate their activities through intricate, mutually dependent chains of biochemical and biophysical signals as cellular processes take place.[12] In order to manipulate cell activity and provide feedback on cell-matrix interaction, scaffolds with precisely adjusted structural, mechanical, and biochemical properties have been constructed.[13] However, immobile scaffolds frequently suffer from a lack of imitating of the dynamic nature of native extracellular matrix. Given their ability to adapt to the change in physiological environment, responsive injectable scaffolds have become powerful substrates that mimic essential attributes of native tissues, allowing for on-demand manipulation of the cell microenvironment.[14] A variety of factors should be taken into account in the rational design of responsive injectable hydrogels for tissue engineering in terms of their biochemical/physical properties. Firstly, biocompatible hydrogel scaffolds that support cell development are required for utilization in biomedical applications. Those that include trapping cells or bioactive substances have to be able to be made into gels without harming the cells or impairing the functions of bioactive substances.[15] The degraded products of hydrogel need to be non-toxic and easily absorbed by human body. The rate of degradation should preferably match the rate of development of new tissue.[16,17] In order to permit diffusion of nutrients and metabolites through the cells and adjacent tissues, the hydrogel needs to possess suitable mass transport features.[18,19] In addition to having the necessary strength and structural stability to endure in *vivo* manipulation, hydrogel scaffolds must also provide a favorable mechanical environment for cell proliferation and differentiation.[20] Since each native tissue has its own strength microenvironment, the mechanical strength of the hydrogel need to fit with corresponding tissues to facilitate the modulation of cellular function and formation of tissue. **Figure 3** summarizes the stiffness of matrix for the proliferation of cells.[21] Therefore, the biological characteristics of hydrogels applied in tissue engineering are just as crucial as their mechanical properties.

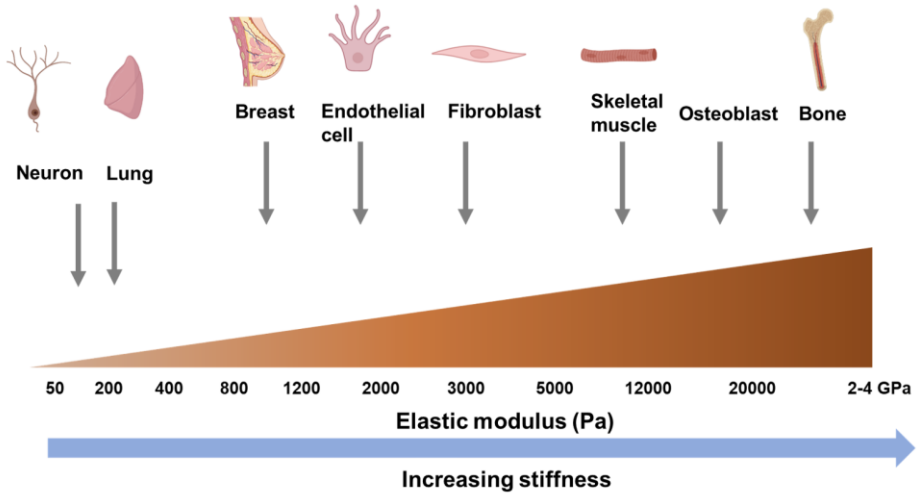

Figure 3. The stiffness of matrix for the proliferation of cells.

In addition to the above-mentioned requirements, the composition of the hydrogel should be matched with the native tissues. For example, the development of hydrogel scaffolds comprised of natural or synthetic polymers and osteo-inductive micro/nano-particles has shown the prospect of bone tissue engineering.[22–26] As an essential part of natural bone, hydroxyapatite ($Ca_{10}(PO_4)_6(OH)_2$) collaborates with collagen type I to offer toughness and avoid bone fractures while it can also trigger osteoblast proliferation and provide the growth and differentiation of mesenchymal stem cells.[27–29] Due to its non-immunogenic feature, biocompatibility, and excellent bone conductivity, hydroxyapatite/polymer composites have been widely used in bone repair.[28] Especially, the fabrication of responsive injectable hydrogels-based scaffolds with constituents of apatite has been a robust approach for the development of bone regeneration.[30–32] Embedding nano-hydroxyapatite into polymer, and inducing apatite formation in simulated body fluid (SBF) are the main way of preparation so far.[33,34] Although responsive injectable hydrogels have been investigated for decades, there are still challenges to realize the clinical application. Therefore, the development of an excellent versatile injectable hydrogel to meet the above-mentioned requirements for tissue engineering applications is urgently needed.

Responsive hydrogels for drug delivery

Responsive hydrogels also can be applied for drug delivery depending on the

different physiological environments in human body. As physical diseases can cause alterations in the microenvironment of the diseased site, such as low pH, raised temperature and varied glucose concentration. For site-specific controlled drug delivery, hydrogels that are responsive to pH, temperature, and enzymes have been taken into consideration.[35] It is generally agreed that solid tumors have extracellular pH values between 6.4-6.8, whereas blood and healthy tissues have pH values between 7.2 and 7.4;[36] the stomach's pH is extremely acidic (range: 1.0 to 2.5), and the small intestine's pH gradually rises from pH 6.0 to pH 7.4 in the terminal ileum.[37,38] Based on the gradient of pH values in human body, a series of pH-responsive hydrogels have been investigated and developed for drug delivery in recent decades. pH-responsive hydrogels involve carboxylic acid and sulfonic acid, ammonium salts, etc. in the gels.[39] Based on the type of side groups, they can be summarized as acidic groups and basic groups. The pH of the conditions is varied, and the extent of dissociation of acidic/basic groups switches as well. This leads to produce a change in the degree of swelling of the hydrogel. The drug release process of pH-responsive hydrogels is depicted in **Figure 4**. Low pH circumstances enable hydrogen bonds to develop in the carboxylic groups of the hydrogel, which reduces the hydrogel's volume for polymers having acidic groups. As a result, such hydrogels with carboxylic groups are incapable of retain additional water in an acidic condition, which inhibits the rate of drug release. However, in an alkaline environment, the hydrogel's volume rises as a result of the electrostatic repulsion in the ionized carboxylic groups. Greater water is taken up by the hydrogel, accelerating the release of the drugs. Conversely, the polymers possessing basic groups, hydrogel will shrink in alkaline environments, but acidic conditions cause them to swell. Because the pH of the environment affects the extent of shrinkage and expansion of hydrogel, it is possible to regulate the rate of drug penetration and release in a hydrogel. A drug-responsive hydrogel that can administer the drug should be able to deliver the ideal dosage to the target spot when required and not release the drug into other parts of the body. Additionally, they need to be capable of spreading out the drug's release over a long time.[40] Although responsive hydrogels have a tremendous amount of potential for specific drug administration, the existing systems are constrained by issues

with burst drug release control, ineffective loading and quick release of hydrophobic drugs, and obstacles achieving prolonged, on-demand, and percussive drug delivery.[41] Accordingly, responsive hydrogels with a controllable behavior need to be designed to fulfill their applications in drug delivery.

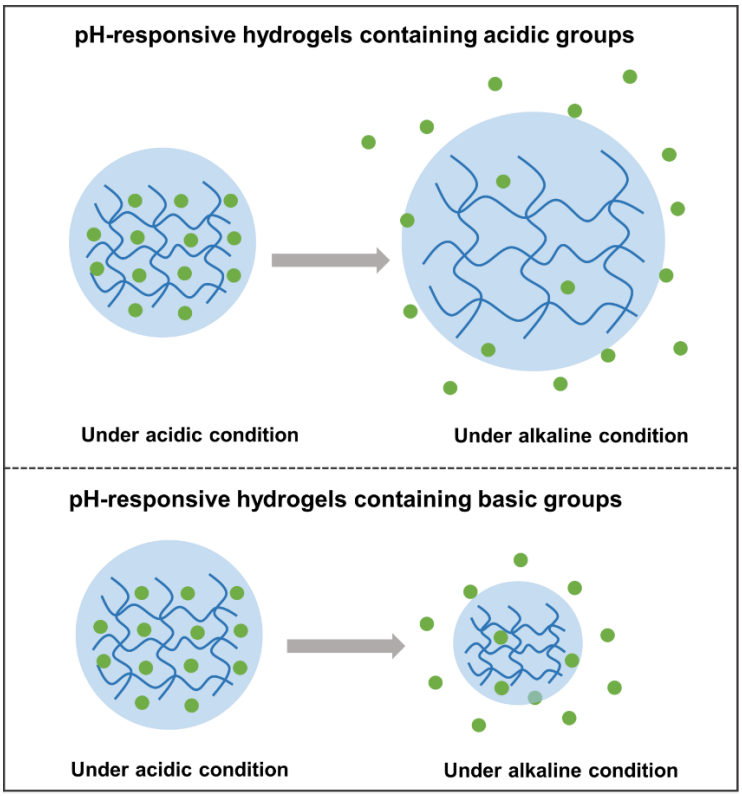

Figure 4. The drug release process of pH-responsive hydrogels.

Natto-derived poly(γ-glutamic acid)

Excellent biomaterials are critical in the development of ideal responsive injectable hydrogels that can serve as scaffolds in biomedical applications. A wide range of biomaterials, both natural and synthetic, have been used to develop hydrogels, including chitosan, collagen or gelatin, alginate, cellulose, hyaluronic acid, polypeptides, heparin, chondroitin sulfate, poly(ethylene glycol), and others.[17] Among various biomaterials, poly(γ-glutamic acid) (PGA) has received much attention for use in different fields because of its favorable properties such as its edibility, nontoxicity, excellent biocompatibility, non-immunogenicity, biodegradability, and extracellular matrix (ECM)-like biomimetic 3D architecture.[42,43] PGA is a naturally occurring homo-polyamide composed of D- and L-glutamic acid units connected by amide bonds

between the α-amino and γ-carboxylic acid groups. The structure and application of PGA are shown in **Figure 5**. PGA can be synthesized by microbial fermentation of different *Bacillus species*. Soybeans are predominantly fermented by *B. subtilis* to yield *natto*, the most widely recognized form of PGA.[44] The carboxylic acid groups on the side chains of PGA not only give pH responsiveness due to the intermolecular interactions of hydrogen bonds but also make it easy to modify. Furthermore, PGA exhibits an outstanding capacity for apatite-forming in SBF, since carboxylic acid groups of PGA are beneficial to heterogeneous apatite nucleation.[45,46] Therefore, PGA composites have been developed for cosmetic, environment, and industrial use, and are also used in health supplements, tissue regeneration and drug delivery.

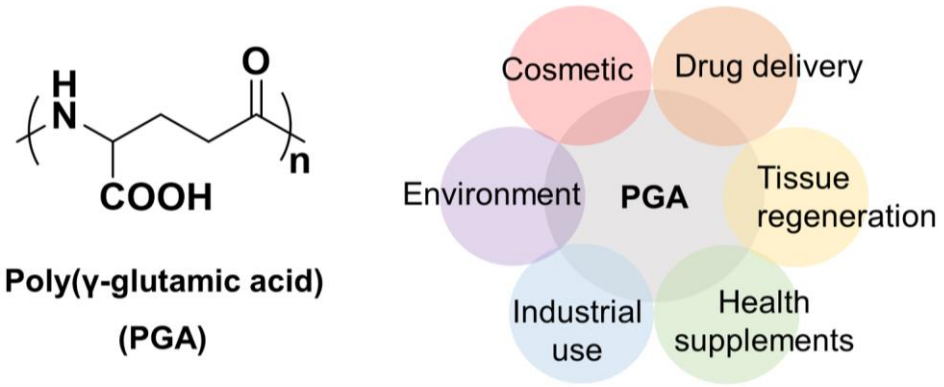

Figure 5. The structure and application of poly(γ-glutamic acid).

In this doctoral dissertation, biocompatible hydrogels using PGA provided by Kookmin University (Seoul, Korea) were prepared to meet the various requirements in biomedical fields, especially in drug delivery and tissue engineering scaffold. According to the use of unique features of PGA (pH responsive property and the ability to induce apatite-forming), muti-functional PGA-based hydrogels were designed and prepared in this research, and then the potential application in drug delivery and tissue engineering scaffold was investigated in detail. **Chapter 1** describes the preparation of pH responsive PGA hydrogels and their potential application in oral drug delivery. **Chapter 2** focuses on the preparation of injectable and adjustable-stiffness PGA hydrogels. The controllable stiffness of PGA hydrogel could match the strength of polymeric matrix for the proliferation of cells, indicating the potential application for

encapsulation of cells. **Chapter 3** studies the effect of addition of calcium ions (Ca^{2+}) into PGA-based hydrogels on the formation of apatite in hydrogels. The design and fabrication strategies of PGA-based hydrogels established in this thesis could provide guidance for the future fabricate polypeptide-based hydrogels.

Outline of this dissertation

The author aimed the development of versatile PGA-based hydrogels for potential biomedical applications. The hydrogels exhibited responsive properties, such as pH responsiveness (**Chapter 1**), temperature and enzymatic responsiveness (**Chapter 2**), and ionic responsiveness (**Chapter 3**). This work is expected to contribute to extending the fundamental research of polypeptide-based hydrogels and their biomedical application, such as tissue engineering and cell/drug delivery.

Chapter 1 Preparation of pH-Responsive Poly(γ-glutamic acid) Hydrogels by Enzymatic Cross-Linking

In this chapter, inspired by the natural nontoxic feature of PGA, a new type of pH-responsive hydrogel comprised of PGA modified with tyramine (PGA-Tyr) was developed through enzymatic cross-linking in the presence of horseradish peroxidase (HRP) and hydrogen peroxide (H_2O_2). The hydrogels possessed good reversibility of pH responsiveness. Indomethacin (IM), a hydrophobic drug model, was encapsulated in the hydrogels by rapid *in situ* gelations. The IM-micelle-loaded hydrogels with a high degree of substitution of PGA-Tyr showed a suppressed burst release behavior in SGF, and sustained drug release in SIF, indicating that PGA-based hydrogels have tremendous promise for oral drug delivery.

Chapter 2 Preparation of Injectable Poly(γ-glutamic acid)-based Biodegradable Hydrogels with Tunable Gelation Rate and Mechanical Strength

In this part of research, in order to develop the injectable hydrogels with adjustable stiffness and biodegradation for the application of tissue scaffolds. A class of injectable

hydrogels was designed using furfuryl amine and tyramine-modified PGA (PGA-Fa-Tyr) and the crosslinker dimaleimide poly(ethylene glycol). The hydrogel could be formed under HRP/H_2O_2 and body temperature stimuli owing to the presence of enzymatic crosslinking and Diels-Alder reaction. The injectable hydrogels displayed controllable mechanical strength, which could be matched with the stiffness of matrix of human tissues. Furthermore, the hydrogel was degraded with proteinase K. These results indicated the hydrogels hold great potential as tissue engineering scaffolds for encapsulating different cell types.

Chapter 3 Preparation of Injectable Poly(γ-glutamic acid)/Chondroitin Sulfate Hydrogels with Mineralization Ability

In Chapter 3, inspired by the inducing apatite-forming ability of PGA, injectable hydrogels were fabricated using hydrazide-modified PGA and oxidized chondroitin sulfate *via* combining acylhydrazone bonds and ionic bonding of carboxylic acid groups or sulfate groups with calcium ions (Ca^{2+}). The resulting hydrogels displayed a fast gelation rate and good self-healing ability owing to the acylhydrazone bonds. The rate of apatite-forming in the hydrogels was greatly promoted in the stimulation of Ca^{2+} ions after immersion in SBF. The hydrogels containing the aldehyde groups possessed good bio-adhesion to the bone tissues. Thus, the hydrogels can serve as a robust template for biomineralization, indicating the potential applicability in bone tissue engineering.

References

1. H. M. El-Husseiny, E. A. Mady, L. Hamabe, A. Abugomaa, K. Shimada, T. Yoshida, T. Tanaka, A. Yokoi, M. Elbadawy and R. Tanaka, *Mater. Today Bio*, **2022**, 13, 100186.
2. Z. Mazidi, S. Javanmardi, S. M. Naghib and Z. Mohammadpour, *Chem. Eng. J.*, **2022**, 134569.
3. Y. Sun, D. Nan, H. Jin and X. Qu, *Polym. Test.*, **2020**, 81, 106283.
4. L. Yu and J. Ding, *Chem. Soc. Rev.*, **2008**, 37, 1473–1481.
5. K. H. Bae, L. S. Wang and M. Kurisawa, *J. Mater. Chem. B*, **2013**, 1, 5371–5388.
6. F. Rizzo and N. S. Kehr, *Adv. Healthc. Mater.*, **2021**, 10, 1–26.
7. H. Uyama and S. Kobayashi, *J. Mol. Catal. B Enzym.*, **2002**, 19, 117–127.
8. M. Kurisawa, J. E. Chung, Y. Y. Yang, S. J. Gao and H. Uyama, *Chem. Commun.*, **2005**, 4312–4314.
9. F. Lee, K. H. Bae and M. Kurisawa, *Biomed. Mater.*, **2015**, 11, 14101.
10. A. P. Mathew, S. Uthaman, K.-H. Cho, C.S. Cho and I.-K. Park, *Int. J. Biol. Macromol.*, **2018**, 110, 17–29.
11. J. A. Yang, J. Yeom, B. W. Hwang, A. S. Hoffman and S. K. Hahn, *Prog. Polym. Sci.*, **2014**, 39, 1973–1986.
12. M. A. Mohamed, A. Fallahi, A. M. A. El-Sokkary, S. Salehi, M. A. Akl, A. Jafari, A. Tamayol, H. Fenniri, A. Khademhosseini and S. T. Andreadis, *Prog. Polym. Sci.*, **2019**, 98, 101147.
13. H. Cao, L. Duan, Y. Zhang, J. Cao and K. Zhang, *Signal Transduct. Target. Ther.*, **2021**, 6, 1–31.
14. C. Mo, R. Luo and Y. Chen, *Macromol. Rapid Commun.*, **2022**, 2200007.
15. X. Xue, Y. Hu, Y. Deng and J. Su, *Adv. Funct. Mater.*, **2021**, 31, 2009432.
16. C. D. Spicer, *Polym. Chem.*, **2020**, 11, 184–219.
17. J. Zhu and R. E. Marchant, *Expert Rev. Med. Devices*, **2011**, 8, 607–626.
18. M. R. Singh, S. Patel and D. Singh, in *Nanobiomaterials in soft tissue engineering*, Elsevier, **2016**, pp. 231–260.
19. C. M. Hwang, S. Sant, M. Masaeli, N. N. Kachouie, B. Zamanian, S.-H. Lee and A. Khademhosseini, *Biofabrication*, **2010**, 2, 35003.
20. S. Santhanam, J. Liang, J. Struckhoff, P. D. Hamilton and N. Ravi, *Acta Biomater.*, **2016**, 43, 327–337.
21. D. T. Butcher, T. Alliston and V. M. Weaver, *Nat. Rev. Cancer*, **2009**, 9, 108–122.
22. K. Matsumura, T. Hayami, S. Hyon and S. Tsutsumi, *J. Biomed. Mater. Res. Part A An Off. J. Soc. Biomater. Japanese Soc. Biomater. Aust. Soc. Biomater. Korean Soc. Biomater.*, **2010**, 92, 1225–1232.
23. Y. Li, C. Liu, W. Liu, X. Cheng, A. Zhang, S. Zhang, C. Liu, N. Li and X. Jian, *Macromol.*

Biosci., **2021**, 21, 2100262.

24. L. Nie, X. Li, P. Chang, S. Liu, Q. Wei, Q. Guo, Q. Wu, L. Fan, O. V. Okoro and A. Shavandi, *Mater. Lett.*, **2022**, 308, 131182.
25. C. Wei, X. Jin, C. Wu and W. Zhang, *J. Mater. Sci. Technol.*, **2022**, 118, 64–72.
26. K. Gkioni, S. C. G. Leeuwenburgh, T. E. L. Douglas, A. G. Mikos and J. A. Jansen, *Tissue Eng. Part B Rev.*, **2010**, 16, 577–585.
27. L. Ghasemi-Mobarakeh, M. P. Prabhakaran, P. Balasubramanian, G. Jin, A. Valipouri and S. Ramakrishna, *J. Nanosci. Nanotechnol.*, **2013**, 13, 4656–4671.
28. R. Florencio-Silva, G. R. da S. Sasso, E. Sasso-Cerri, M. J. Simões and P. S. Cerri, *Biomed Res. Int.* **2015**, 421746.
29. M. Pilia, T. Guda and M. Appleford, *Biomed Res. Int.* **2013**,458253.
30. E. Ho, A. Lowman and M. Marcolongo, *J. Biomed. Mater. Res. Part A An Off. J. Soc. Biomater. Japanese Soc. Biomater. Aust. Soc. Biomater. Korean Soc. Biomater.*, **2007**, 83, 249–256.
31. Y. Li, H. Y. Yang and D. S. Lee, *J. Control. Release*, 2021, 330, 151–160.
32. S. Y. Kim and S. C. Lee, *J. Appl. Polym. Sci.*, **2009**, 113, 3460–3469.
33. A. Mellati and J. Akhtari, *Res. Mol. Med.*, **2019**, 1–14.
34. S. Iftikhar, S. Zahid, S. Z. Safi, A. F. Khan, M. Nawshad, S. Ghafoor, A. S. Khan and A. T. Shah, *Mater. Sci. Eng. C*, **2020**, 113, 110956.
35. A. Raza, T. Rasheed, F. Nabeel, U. Hayat, M. Bilal and H. Iqbal, *Molecules*, **2019**, 24, 1117.
36. Y. Wang, K. Zheng, G. Xuan, M. Huang and J. Xue, *Int. J. Nanomedicine*, **2018**, 13, 7681.
37. Z. Liu and N. Zhang, *Curr. Pharm. Des.*, **2012**, 18, 3442–3451.
38. K.Y. Cheng, S.C. Tsai and W.-Y. Lin, *Eur. J. Nucl. Med. Mol. Imaging*, **2003**, 30, 907–911.
39. F. Ofridam, M. Tarhini, N. Lebaz, É. Gagnière, D. Mangin and A. Elaissari, *Polym. Adv. Technol.*, **2021**, 32, 1455–1484.
40. J. F. Coelho, P. C. Ferreira, P. Alves, R. Cordeiro, A. C. Fonseca, J. R. Góis and M. H. Gil, *EPMA J.*, **2010**, 1, 164–209.
41. J. Li and D. J. Mooney, *Nat. Rev. Mater.*, **2016**, 1, 1–17.
42. S. Bin Park, M. H. Sung, H. Uyama and D. K. Han, *Prog. Polym. Sci.*, **2021**, 113, 101341.
43. O. A. Balogun-agbaje, O. A. Odeniyi and M. A. Odeniyi, *Future Journal of Pharmaceutical Sciences*, **2021**, *7*(1), 1-10 .
44. L. C. Johnson, A. T. Akinmola and C. Scholz, *Biocatal. Agric. Biotechnol.*, **2022**, 40, 102292.
45. T. Miyazaki, J. Mukai, E. Ishida and C. Ohtsuki, *Biomed. Mater. Eng.*, **2013**, 23, 339–347.
46. A. Sugino, T. Miyazaki and C. Ohtsuki, *J. Mater. Sci. Mater. Med.*, **2008**, 19, 2269–2274.

Chapter 1.

Preparation of pH-responsive poly(γ-glutamic acid) hydrogels by enzymatic crosslinking

1.1 Introduction

Oral medication is the most common form of drug administration because of the convenience of drug administration *via* the oral route, patient preference, cost effectiveness, and ease of large-scale manufacturing.[1] In recent years, there has been an increasing amount of research on pH-responsive hydrogels because they can generate volume or phase transition under different physiological conditions, achieving the release of drug in target sites.[2–5] Currently, various polymers, which can be classified as cationic, anionic and amphiphilic types, have been employed to prepare pH-responsive hydrogels for oral delivery systems.[6] Poly(γ-glutamic acid) (PGA) is a safe, non-toxic and edible *natto*-derived biomaterial that is formed by an amide linkage between the α-amino and γ-carboxyl groups of two glutamic acids; it is naturally synthesized by *Bacillus subtilis*.[7] The carboxylic acid groups on the side chains of PGA not only endow it with pH responsiveness due to the intermolecular interactions of hydrogen bonds, but they are also amenable to modification.[8,9] Additionally, the amine group in the N-terminal γ-glutamic unit can be recognized by γ-glutamyl transpeptidase in the enterocytes of the small intestine, thus contributing to oral drug delivery.[10] Recently, considerable effort has been dedicated to designing and developing PGA-based hydrogels for biomedical applications. Park et al. prepared pH-sensitive PGA/chitosan hydrogels, which swelled under acidic conditions (pH 1.0-3.0), while they dramatically shrank above pH 6.0, thus presenting promise for application in oral drug delivery systems.[11] Yang et al. synthesized biodegradable hydrogels based on poly(ethylene glycol) methacrylate-graft-PGA and poly(ethylene glycol) dimethacrylate via photoinduced polymerization. The hydrogels showed excellent pH-responsive swelling and biodegradation behaviors.[12] Ma et al. fabricated injectable

hydrogels using methacrylate-functionalized hyaluronic acid and PGA *via* photopolymerization; a weak burst release behavior was observed when the drug was encapsulated in this hydrogel.[13] Although biocompatible PGA-based hydrogels for drug delivery have been developed using different preparation approaches, some chemical reactions involve toxic initiators, catalysts, or solvents, which are harmful to the human body.

Enzymatic cross-linking has been paid increasing attention to prepare hydrogels, because of the mild reaction conditions, non-toxicity, tunable gelation rate, and mechanical properties.[14–18] Notably, drugs or proteins can be effectively encapsulated in hydrogels during the *in situ* enzymatic crosslinking process, thus providing a convenient route for drug loading.[19] Previously, our group prepared hyaluronic acid hydrogels *via* enzymatic crosslinking. The gelation time and mechanical properties of this hydrogel could be easily controlled by changing the concentrations of horseradish peroxidase (HRP) and hydrogen peroxide (H_2O_2).[16] To the best of our knowledge, although there are studies about PGA-based hydrogels formed by enzymatic crosslinking,[20–24] pH responsiveness and drug release of hydrogels via this facile method have not been explored for oral drug delivery. Currently, the main obstacles in the development of hydrogels for oral drug delivery are the difficulties in reducing the adverse side effects of drug release and in improving drug absorption,[25,26] which restrict their practical application. Based on these considerations, PGA-based hydrogels prepared by enzymatic crosslinking were proposed to encapsulate drug micelles for application in oral drug release to reduce the side effects of drugs in the gastric environment.

In this study, inspired by the natural non-toxic feature of PGA, hydrogel based on PGA grafted with tyramine (PGA-Tyr) was prepared in the presence of HRP and H_2O_2. The chemical structure of PGA-Tyr was characterized by attenuated total reflection Fourier transform infrared (ATR-FTIR) spectroscopy and ^{1}H NMR. The gelation time, storage modulus, swelling behavior, and pore size, were explored in detail by tuning HRP and H_2O_2 concentrations or the degree of substitution (DS) of PGA-Tyr. The pH

responsiveness of the hydrogels was investigated by measuring the swelling ratio in solutions with various pH values. The biodegradation behavior of the hydrogels was studied under simulated physiological conditions. Moreover, the hydrophobic drug or drug micelles were encapsulated in hydrogels during *in situ* enzymatic crosslinking. The release behaviors of the pure drug and drug micelles in hydrogels were studied *in vitro*.

1.2 Experimental

Materials

Poly(γ-glutamic acid) (PGA, M_n = 1.2 × 10^5 g/mol) (Seoul, Korea). Tyramine hydrochloride (Tyr), horseradish peroxidase (HRP, 100 U/mg), hydrogen peroxide (H_2O_2), pepsin from porcine stomach, and trypsin from porcine pancreas were purchased from Wako Chemicals (Osaka, Japan). 1-(3-dimethylaminopropyl)-3-ethylcarbodiimide hydrochloride (EDC) and N-hydroxysuccinimide (NHS) were purchased from Tokyo Chemical Industry (Tokyo, Japan). 2-morpholinoethanesulfonic acid (MES), indomethacin (IM), and pluronic F-127 (PF127) were purchased from Sigma-Aldrich (St. Louis, MO, USA). All reagents were used without further purification.

Synthesis of PGA-Tyr

PGA (1.29 g, 10 mmol) was dissolved in 100 mL of MES buffer (0.1 mol/L, pH 5.5). Then, EDC (0.96 g, 5 mmol; 1.92 g, 10 mmol) and NHS (0.58 g, 5 mmol; 1.15 g, 10 mmol) were added to activate the carboxylic groups for 30 min. Next, Tyr (0.87 g, 5 mmol (DS1); 1.73 g, 10 mmol (DS2) was added to the solution. The mixture was kept at room temperature for 12 h under stirring. After the reaction, the mixture was added dropwise to a large excess of ethanol to form a precipitate. The precipitated product was dialyzed against a 0.1 mol/L NaCl solution for 2 d and deionized water for 3 d using a dialysis membrane with a molecular weight cut-off (MWCO) of 1000. A white spongy product, PGA-Tyr, was obtained by lyophilization (**Scheme 1-1**).

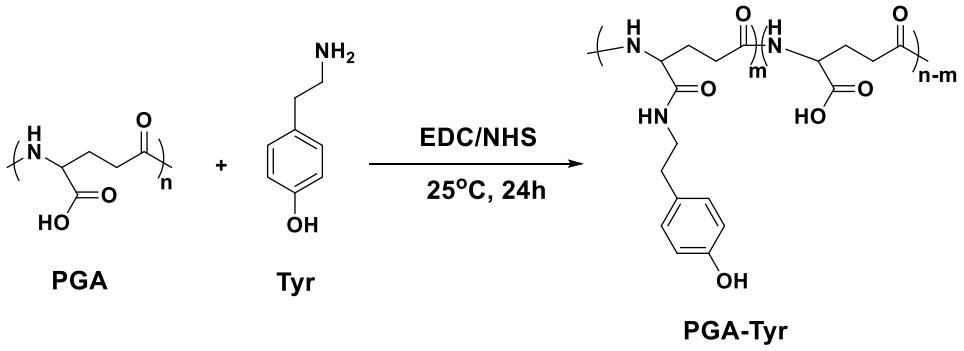

Scheme 1-1. Synthesis of PGA-Tyr.

Characterization of PGA-Tyr

ATR-FTIR spectroscopy (Thermo Scientific Nicolet iS 5, USA) was used to confirm the presence of the phenol groups of PGA-Tyr. A lyophilized PGA-Tyr sample was characterized by ^{1}H-NMR (Bruker AVANCE 400 MHz, Germany) with D_2O as the solvent. The DS was determined by comparing the integrated areas under the proton peaks at 6.61 and 6.91 ppm to that of the peak at 3.96 ppm. The calculation of DS is shown below (**Equation 1.1**).

$$DS = \frac{Area(6.61\ ppm)+Area(6.91\ ppm)}{Area(3.96\ ppm)\times 4} \times 100\% \quad (1.1)$$

Hydrogel formation

PGA-Tyr (48 mg) was dissolved in 1.95 mL of phosphate-buffered saline (PBS, pH 7.0) in a vial. Freshly prepared HRP and H_2O_2 solutions (H_2O_2/Tyr molar ratio = 0.125, 0.25, 0.5, 1.0, and 2.0) were added to the vial, which was gently vortexed. The vial inverting method was used to measure the gelation time of the hydrogels, which was defined as the time when no visual flow was observed within 30 s after inverting the vial at room temperature.[16,21,27] The gelation times were measured in triplicate, and the values were averaged. The synthetic route for the hydrogels is shown in **Scheme 1-2**. The final PGA-Tyr concentration was 2.4% (w/v). The hydrogels prepared with DS1 (5%) and DS2 (10%) of PGA-Tyr were named Eny5 and Eny10, respectively. The formulations of the prepared hydrogels are presented in **Table 1-1**.

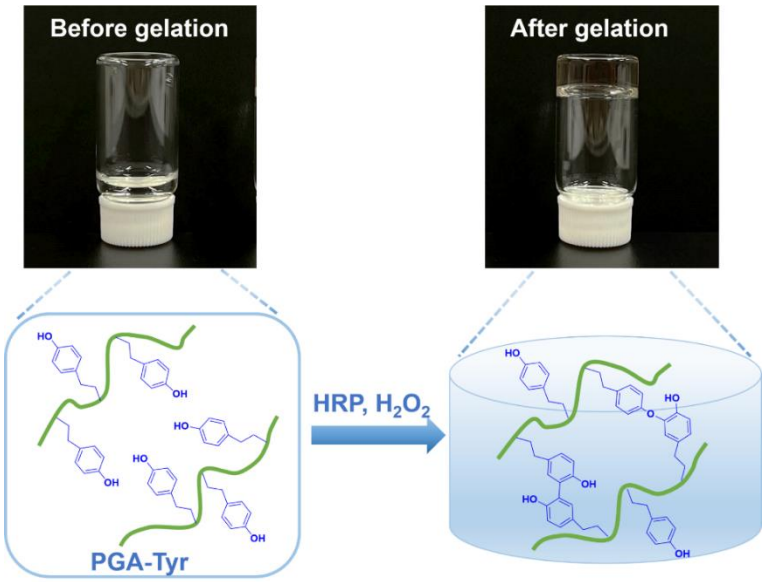

Scheme 1-2. Schematic of the hydrogel formation process.

Table 1-1. Formulations of the prepared hydrogels.

Sample	DS of PGA-Tyr [a] (%)	HRP (U/mL)	H_2O_2/Tyr (mol/mol)	Polymer concentration (%)
Eny5 hydrogel	5	0.5, 2.5, 5.0, 10, 15	0.125, 0.25, 0.5, 1, 2	2.4
Eny10 hydrogel	10			2.4

[a] DS is the degree of substitution which was determined by ^{1}H NMR.

Rheological behavior

Rheological analyses of the hydrogels were performed using a Hakke Rheostress 6000 (Thermo Scientific, USA) equipped with 20 mm diameter parallel plates. The prepared cylindrical hydrogels (diameter 13.0 mm, height 5.0 mm) were placed on the bottom of the parallel plates. The oscillation frequency sweep was conducted from 0.1 to 1 Hz at 0.1% strain and 25 °C to determine the moduli of the hydrogels.

pH responsiveness

To evaluate the reversibility of their pH responsiveness, the hydrogels were immersed in PBS (pH 7.0) at 37 °C for 3 h to reach equilibrium swelling. The weight of the samples was measured, and the swelling ratio was calculated using Equation (1). Then, the swollen samples were quickly transferred to an acidic solution with pH 2.0, in which they exhibited deswelling behavior. After 1 h, the samples were removed from the acidic solution, and the weight (W_t) was measured after blotting the excess water on the surface of the hydrogels using filter paper. The swelling ratio after immersion in the acidic solution was calculated using **Equation 1.2**. The samples were transferred back to PBS (pH 7.0) for 1 h of swelling and weighed again. This cycle (swelling for 1 h in PBS and deswelling for 1 h in an acidic solution) was repeated several times to determine the deswelling–swelling kinetics of the hydrogels.

$$Swelling\ ratio = \frac{W_t}{W_0} \quad (1.2)$$

Morphology

Morphologies of the hydrogels were characterized using scanning electron microscopy (SEM) (Hitachi SU3500, Japan). The hydrogels were frozen with liquid nitrogen about 30 min and cut with a razor to obtain cross sections, then lyophilized for 24 h and sputtered with gold by using an MSP-1S magnetron sputter (Vacuum Device Inc., Japan). The samples were observed under high vacuum at an accelerating voltage of 1.50 kV.

***In vitro* degradation**

Hydrogel samples were lyophilized and weighed (W_{l1}), then the samples were submerged in 25ml of simulated gastric fluid (SGF, 0.1 mol/L PBS-HCl, pH 2.0) with pepsin (3 mg/mL), and simulated intestinal fluid (SIF, 0.1 mol/L PBS, pH 7.0) with trypsin (10 mg/mL), respectively, to evaluate the degradation behaviors. At selected time points, the samples were removed and lyophilized again to obtain the dried mass (W_{l2}). The pepsin and trypsin solutions were replaced in each sample at each time point

with a fresh solution. The remaining mass of the hydrogels was defined by the following equation (**Equation 1.3**):

$$Remaining\ mass = \frac{W_{l2}}{W_{l1}} \quad (1.3)$$

The degradation experiments were performed in triplicate and the values were averaged.

Drug encapsulation and *in vitro* release

IM was employed as a hydrophobic drug model in this study to investigate *in vitro* release. First, IM (10.0 mg) and PF127 (40.0 mg) were dissolved in 1.95 mL of PBS (pH 7.0) and stirred for 24 h to form a stable drug micelle solution; then, PGA-Tyr (48 mg) was added to the solution. After this solution was mixed homogenously, HRP and H_2O_2 were added to form indomethacin-loaded hydrogels. To explore the influence of PF127 on drug release, hydrogels encapsulating solely IM without PF127 were selected as the control group. Hydrogels loaded with IM and IM micelles were incubated in a bio-shaker at 37 °C for 12 h before use.

To study the drug release profile in simulated gastrointestinal conditions, SGF and SIF with pH values of 2.0 and 7.0 were selected to test the drug release behaviors. IM-loaded hydrogels were first incubated in 10 mL of an acidic solution (pH 2.0) at 37 °C for 1 h. Subsequently, the samples were transferred into 10 mL of PBS (pH 7.0) at 37 °C for 3 h. At various times, 2.0 mL of the incubated solution was removed and replaced with an equal volume of the corresponding fresh solution. The amount of IM released into the medium was quantified by using a UV spectrophotometer (Synergy HT SIAFR-4, USA) to measure the absorbance of the drug at 320 nm and then calculating the standard curve equations in different pH solutions.

The drug loading efficiency and cumulative release of the drug-loaded hydrogel were calculated as follows (**Equations 1.4** and **1.5**, respectively):

$$Loading\ efficiency = \frac{m_1 - m_2}{m_0} \times 100\% \quad (1.4)$$

$$Cumulative\ release = \frac{V_0 C_n + V\Sigma C_{n-1}}{m_e} \times 100\% \quad (1.5)$$

where m_1 is the total mass of the drug, m_2 is the mass of the drug that remains in the total collected solution after washing the surface of the hydrogels, and m_0 is the mass of the dried hydrogels. C_n and C_{n-1} are the drug concentrations at times n and n-1, respectively, V_0 is the initial volume of the drug release medium, V is the sampling volume, and m_e is the drug mass loaded into the hydrogels.

1.3 Results and Discussion

Characterization of PGA-Tyr

PGA-Tyr was prepared by the modification of PGA with tyramine using EDC/NHS as condensation reagents. The characteristic peaks of phenol groups can be observed at 6.61 and 6.91 ppm in the ^{1}H-NMR spectra in **Figure 1-1**. The DS was calculated by comparing the integrated areas of the phenol group peaks with the area of the proton peak assigned to the α-carbon of glutamic acid (1H, α-CH–) at approximately 3.96 ppm. The DS values of PGA-Tyr were 5.0% (DS1) and 10.0% (DS2). The ^{1}H-NMR spectra proved the successful grafting of phenol groups onto the PGA backbone.

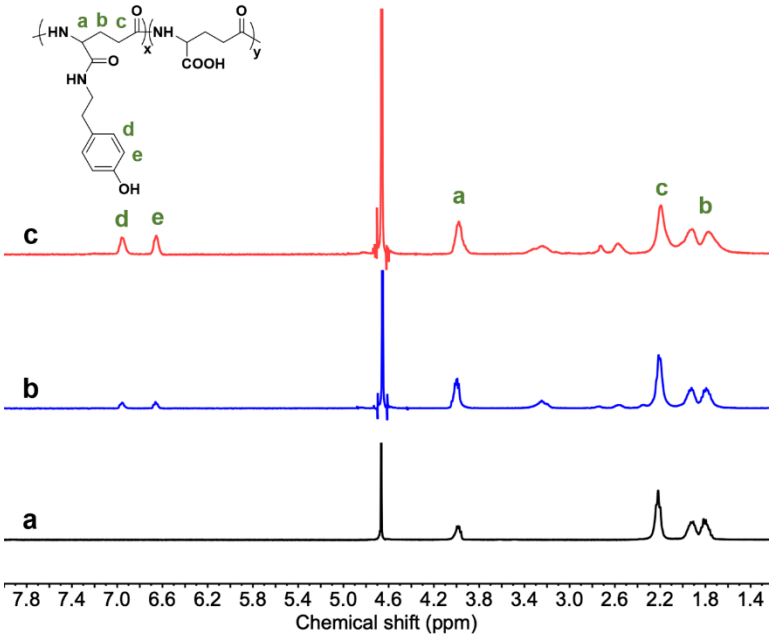

Figure 1-1. ^{1}H-NMR spectra of PGA (a), PGA-Tyr (b) and (c) in D_2O.

Gelation time of the hydrogels

Hydrogels were prepared through the enzymatic crosslinking of tyramine moieties by H_2O_2 and HRP, and the gelation time was determined using the vial tilting method. The dependence of the gelation time on the HRP and H_2O_2 concentrations is shown in **Figure 1-2**. The gelation times of the Eny5 and Eny10 hydrogels decreased substantially from 160 to 38 s and from 30 to 10 s, respectively, as the HRP concentration increased from 0.5 to 15.0 U/mL at a fixed H_2O_2/Tyr molar ratio of 0.5. This could be because increasing the HRP concentration accelerated the rate of generation of phenol free radicals, leading to a faster gelation rate. However, when the HRP concentration reached 10.0 and 5.0 U/mL for the Eny5 and Eny10 hydrogels, respectively, the decrease in gelation time reached a plateau, indicating excessive HRP did not further promote gelation of the hydrogels. Furthermore, as the H_2O_2/Tyr molar ratio increased from 0.125 to 0.5, the gelation time gradually decreased from 180 to 148 s and from 40 to 15 s for the Eny5 and Eny10 hydrogels, respectively, when the HRP concentration was 2.5 U/mL. In contrast, an almost constant or slightly prolonged gelation time was observed when the H_2O_2/Tyr molar ratio was above 0.5 because excessive H_2O_2 inhibited the activity of HRP. In addition, compared with the fast gelation time of the Eny10 hydrogels, longer periods were required for the gelation of the Eny5 hydrogels when the HRP concentration and H_2O_2/Tyr molar ratio remained constant owing to the high concentration of tyramine groups in the Eny10 hydrogels. Therefore, the gelation time of hydrogels can be tuned by changing the concentrations of HRP and H_2O_2 or the DS of PGA-Tyr.

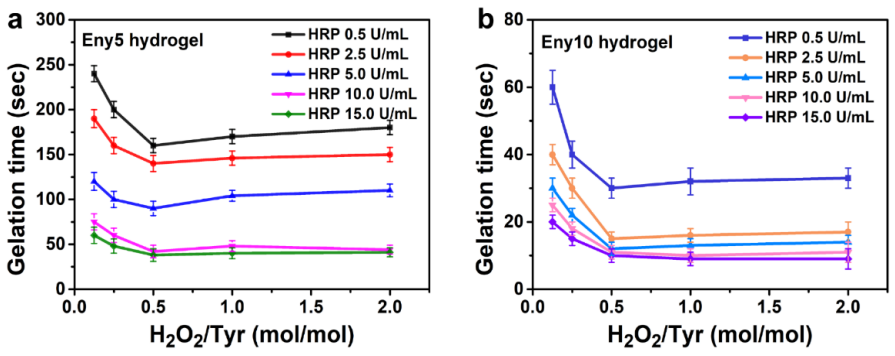

Figure 1-2. Dependence of gelation times on the HRP and H_2O_2 concentrations.

Rheological behavior of the hydrogels

To investigate the effects of the H_2O_2 and HRP concentrations on the properties of the hydrogels, the storage modulus (G') of the hydrogels was measured under a frequency sweep. **Figure 1-3** shows the effect of H_2O_2 concentration on the G' of the hydrogels formed by enzymatic crosslinking at a fixed frequency (f = 1 Hz); the HRP concentration was fixed at 2.5 U/mL. The G' values of the Eny5 and Eny10 hydrogels increased significantly from 200 to 1600 Pa and from 5100 to 17300 Pa as the H_2O_2/Tyr molar ratio increased from 0.125 to 0.5. According to the mechanism of enzymatic crosslinking, the quantity of tyramine groups that actually participated in the crosslinking reaction would depend on the amount of available H_2O_2. The higher H_2O_2/Tyr molar ratio implied that more phenol groups participated in the crosslinking reaction, which resulted in a more highly crosslinked network and a higher mechanical strength. However, the G' values of the hydrogels decreased markedly when the H_2O_2/Tyr molar ratio was above 0.5. This is attributed to inactivation of the enzyme in the presence of excessive H_2O_2.[27–29] Therefore, a H_2O_2/Tyr molar ratio of 0.5 was chosen to prepare the hydrogels in the following studies.

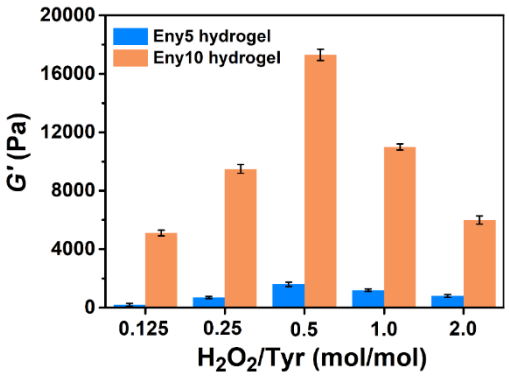

Figure 1-3. Storage modulus of hydrogels (HRP: 2.5 U/mL).

Subsequently, the effect of HRP concentration on the storage modulus of the hydrogels was investigated when the H_2O_2/Tyr molar ratio was fixed at 0.5. As shown in **Figure 1-4**, the G' values of the Eny5 hydrogels visibly increased from 300 to 2700 Pa as the HRP concentration increased from 0.5 to 10.0 U/mL. This was because the rate of generation of phenol radicals increased with increasing HRP concentration,

leading to a high mechanical strength. However, when the HRP concentration increased to 15 U/mL, the G' value decreased, indicating that excessive HRP did not enhance the crosslinking of the hydrogels. Note that the G' values of the Eny10 hydrogels reached a maximum value (~17300 Pa) with 2.5 U/mL of HRP, and then declined dramatically at higher HRP concentrations. This demonstrates that the mechanical properties of the hydrogels were related to the HRP concentration. When the H_2O_2/Tyr molar ratio was constant, a low HRP concentration formed strong Eny10 hydrogels, while hard Eny5 hydrogels required a high HRP concentration. Therefore, in this study, the satisfactory HRP concentrations for the Eny5 and Eny10 hydrogels were 10 and 2.5 U/mL, respectively, which yielded hydrogels with higher storage moduli at the same H_2O_2/Tyr ratio.

Furthermore, the DS of PGA-Tyr also affected the strength of the hydrogels. When the H_2O_2/Tyr molar ratio was 0.5, the maximum G' value of the Eny10 hydrogel with 2.5 U/mL of HRP was 17300 Pa, which was higher than that of the Eny5 hydrogel with 10.0 U/mL of HRP (~2700 Pa). It is worth noting that the maximum G' value of the Eny10 hydrogels was approximately an order of magnitude larger than that of the Eny5 hydrogels. This was because the PGA-Tyr with a higher DS formed a more highly crosslinked network, resulting in hydrogels with a higher mechanical strength. The strength of the hydrogels was also related to the gelation time: the shorter the gelation time, the higher the G' value, which was in agreement with the results previously reported by our group.[16] Based on the above results, the mechanical properties of hydrogels could be regulated by the HRP and H_2O_2 concentrations, as well as the DS of PGA-Tyr. The optimum conditions for the Eny5 and Eny10 hydrogels were 10.0 and 2.5 U/mL of HRP with a fixed H_2O_2/Tyr molar ratio of 0.5, which were selected for the following investigation.

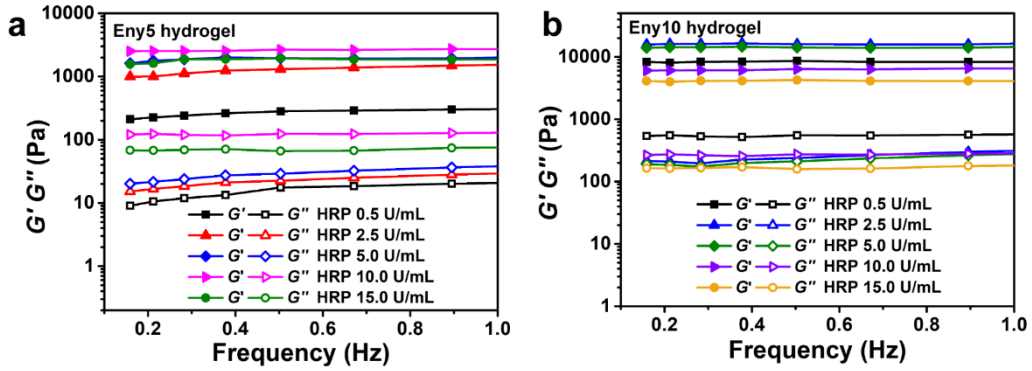

Figure 1-4. Storage (*G'*) and loss (*G''*) moduli of (a) Eny5 and (b) Eny10 hydrogels under a frequency sweep (H_2O_2/Tyr molar ratio: 0.5).

pH-responsiveness of the hydrogels

The pH responsiveness of the hydrogels was evaluated using the swelling ratios in solutions with different pH values (**Figure 1-5a**). The swelling ratios of the Eny10 hydrogel in pH 7.0, 8.0, and 9.0 solutions were 38.0, 36.1, and 34.9, respectively, whereas the swelling ratios in acidic solutions, such as pH 2, decreased considerably to 4.9. A similar variation in the swelling behavior was observed for the Eny5 hydrogel in different pH solutions. In addition, the Eny5 and Eny10 hydrogels exhibited the lowest swelling ratios at pH 2.0. This was because when the hydrogels soaked in a solution with a pH that was lower than the pKa of PGA (2.6-3.6),[8,9] the protonation of –COOH in PGA occurred. The protonation of –COOH can cause the formation of hydrogen bonds between –COOH, which would make the PGA chains tighter and less hydrophilic. In contrast, hydrogels had higher swelling ratios in solutions with a pH above 7.0. This was due to the deprotonation of –COOH in neutral and basic solutions, where the electrostatic repulsion between $–COO^-$ caused PGA chains to become looser and more hydrated. Upon a change in pH, the protonation/deprotonation of –COOH in the hydrogels altered the hydrogen bonding between –COOH and consequently affected the swelling behavior of the hydrogels. Because of the above reasons, the Eny10 hydrogel barely swelled and shrunk in a pH 2.0 solution compared to the original one, while it swelled remarkably after immersion in a pH 7.0 solution (**Figure 1-5c**). According to the SEM images in **Figure 1-5d-f**, the lyophilized Eny10 hydrogel shrunk

under acidic conditions exhibited a more compact pore size than that of the original lyophilized Eny10 hydrogel, whereas the lyophilized hydrogel swollen under neutral conditions displayed a looser pore size.

Subsequently, pH 2.0 and 7.0 solutions were selected for SGF and SIF, respectively to explore the reversibility of the pH responsiveness (**Figure 1-5b**). First, the hydrogels were soaked in a pH 7.0 solution to reach equilibrium swelling. Then, the swollen hydrogels were quickly transferred to a pH 2.0 solution. The Eny10 hydrogel not only displayed a smaller variation in swelling between pH 2.0 and 7.0 solutions compared to that of the Eny5 hydrogel, but it also exhibited a more stable swelling value. This could be attributed to the larger number of phenol groups in the Eny10 hydrogel, which led to a high crosslinking density in the hydrogel. Therefore, pH-responsive PGA-based hydrogels are viable candidates for colon-targeted drug delivery systems.

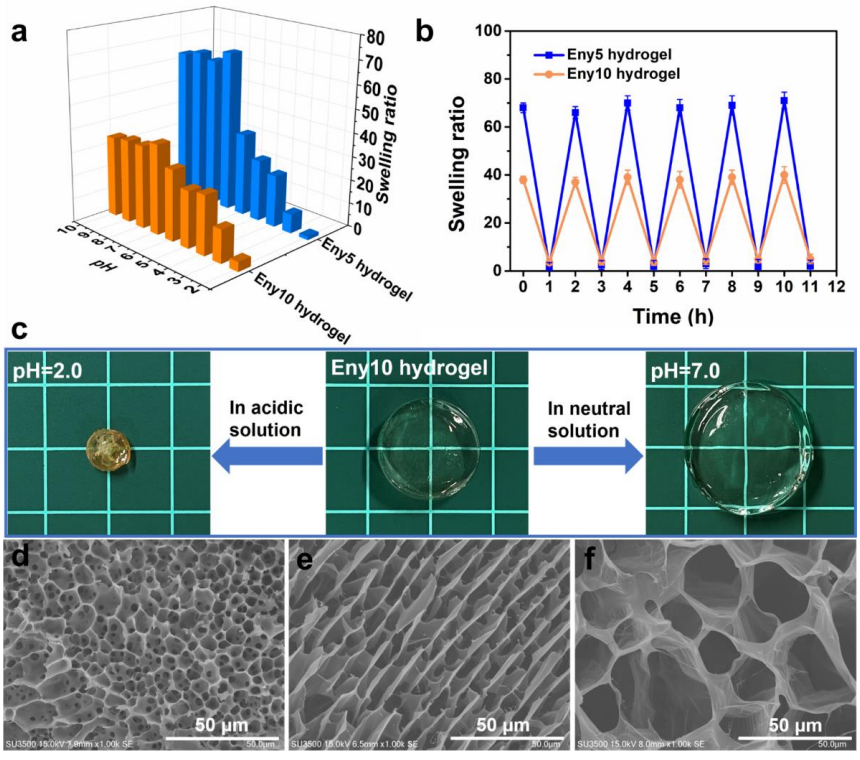

Figure 1-5. (a) Swelling ratios of the hydrogels in various pH solutions; (b) Reversibility of the pH responsiveness of the hydrogels; and (c) Images of the Eny10 hydrogel; SEM images of the lyophilized Eny10 hydrogel (d) in pH 2.0 solution, (e) without immersion, and (f) in pH 7.0 solution.

In vitro degradation of the hydrogels

Biodegradation properties of hydrogels strongly affect biomedical applications, especially with respect to controlled drug delivery. Here, biodegradation behavior of the Eny5 and Eny10 hydrogels was studied under simulated physiological conditions as shown in **Figure 1-6**. The hydrogels were gradually degraded within the 8 h due to the presence of pepsin and trypsin. Compared with Eny5 hydrogel, Eny10 hydrogel degraded slowly in both SGF and SIF, and the weight loss was not exceeded 30% for 8 h. This result was ascribed to the fact that the Eny10 hydrogel with a higher more phenol groups had a higher crosslinking density. Moreover, the degradation rate of the hydrogels incubated in SIF was higher than that of hydrogels in SGF, which was related with the solutions with different pH values. As above described, the hydrogels showed obviously pH-responsiveness due to the protonation/deprotonation of –COOH of PGA. The hydrogels shrunk owing to the less hydrophilic of PGA under SGF, which leaded to a limited degradation tendency. On the contrary, the swollen hydrogels under SIF were prone to degradation because of more hydrophilic of PGA. It is worth noting that the degradation products of PGA have no cytotoxicity.[30] Therefore, the hydrogels displayed excellent pH-dependent degradation behavior, which have a critical role in oral drug delivery systems.

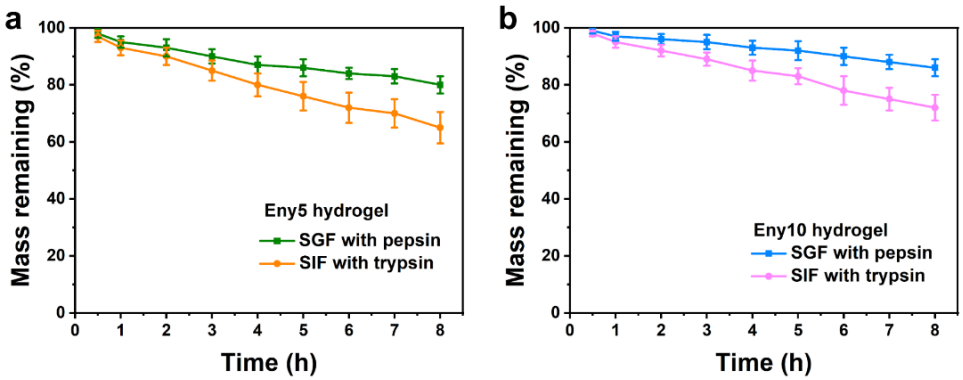

Figure 1-6. Degradation profiles of (a) Eny5 and (b) Eny10 hydrogels in SGF with pepsin and SIF with trypsin, respectively.

In vitro drug release of the hydrogels

Controlled-release delivery of hydrophobic drugs based on the solution pH is important for oral drug delivery. To test drug release in the gastrointestinal tract (GIT) environment, hydrogel-encapsulated drugs were tested in a pH 2.0 solution for 1 h and then in a pH 7.0 for 3 h to mimic SGF and SIF, respectively. Here, IM was utilized as a hydrophobic drug model, which was encapsulated in the hydrogels *in situ* during enzymatic crosslinking. **Figure 1-7** shows the drug-loading efficiencies of the hydrogels. The loading efficiency of the Eny10 hydrogel was higher than that of the Eny5 hydrogel, suggesting that the higher effective crosslinking density of the Eny10 hydrogel allowed a larger amount of drug to be encapsulated. In addition, drug micelles comprising IM entrapped in PF127 were explored. The loading efficiencies of the Eny5 and Eny10 hydrogels loaded with pure IM and IM micelles improved from 5.2% to 8.7% and from 14.5% to 19.1%, respectively, indicating that the format of the drug (whether IM was pure or in micelles) noticeably affected the loading efficiency. Therefore, mixing IM with PF127 (a non-ionic surfactant useful for solubilizing hydrophobic molecules) formed drug micelles, which had better water solubility than that of pure hydrophobic IM.

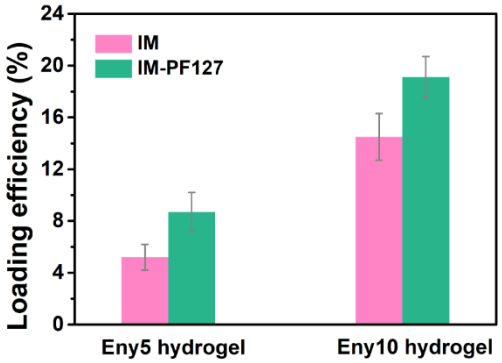

Figure 1-7. Loading efficiencies of hydrogels loaded with pure IM and IM with PF127.

The cumulative release of the hydrogels loaded with pure IM and IM micelles in the GIT environment was investigated (**Figure 1-8)**. The drug-loaded hydrogels exhibited moderate drug release in SGF (pH 2.0) and higher release in SIF (pH 7.0). The hydrogels demonstrated clear pH-dependent drug release behavior, which is consistent

with the swelling behavior in solutions with different pH values. **Figure 1-8c** displays the drug release process under acidic and neutral conditions. The reduced drug release in an acidic environment is related to the shrinkage of hydrogels with a low swelling ratio. However, when transferred to a neutral environment, the hydrogels exhibited a higher swelling ratio, resulting in the rapid release of a large amount of the drug. As shown in **Figure 1-8a**, the Eny5 hydrogel loaded with pure IM in SGF exhibited a burst release (~63.3%), which was related to the degree of shrinkage of the hydrogel in an acidic environment (pH 2.0), as described above. A greater shrinkage of the hydrogel resulted in a greater release of the drug. This is not favorable for the absorption of drugs in the intestinal environment because most drugs are released in the gastric environment. The release of the Eny5 hydrogel loaded with IM micelles decreased to 50.8% under the same conditions, implying that IM micelles improved the stability of drug release in acidic environments. As shown in **Figure 1-8b**, the release of the Eny10 hydrogel loaded with pure IM in SGF was 40.0%, whereas the release of the Eny10 hydrogel loaded with IM micelles in SGF decreased significantly to 18.6%, indicating that in addition to the IM micelles, the high crosslinking density of the Eny10 hydrogel effectively prevented detrimental drug release in SGF. Moreover, the drug release of the hydrogels in SIF was markedly higher than that in SGF owing to the higher swelling behavior in neutral solutions. The final release for the Eny10 hydrogels loaded with pure IM and IM micelles were 81.6% and 85.4%, respectively, suggesting that IM micelles did not affect the release of the drug in SIF. In addition, it is noted that the Eny10 hydrogel loaded with IM micelles displayed a high drug loading capacity, weak and steady release behavior in SGF, and sustained drug release in SIF, which should decrease the adverse side effects of drug release in the gastric environment and promote drug absorption in the intestinal environment. Therefore, the pH responsiveness of hydrogels makes them good candidates for site-specific drug delivery in the intestine.

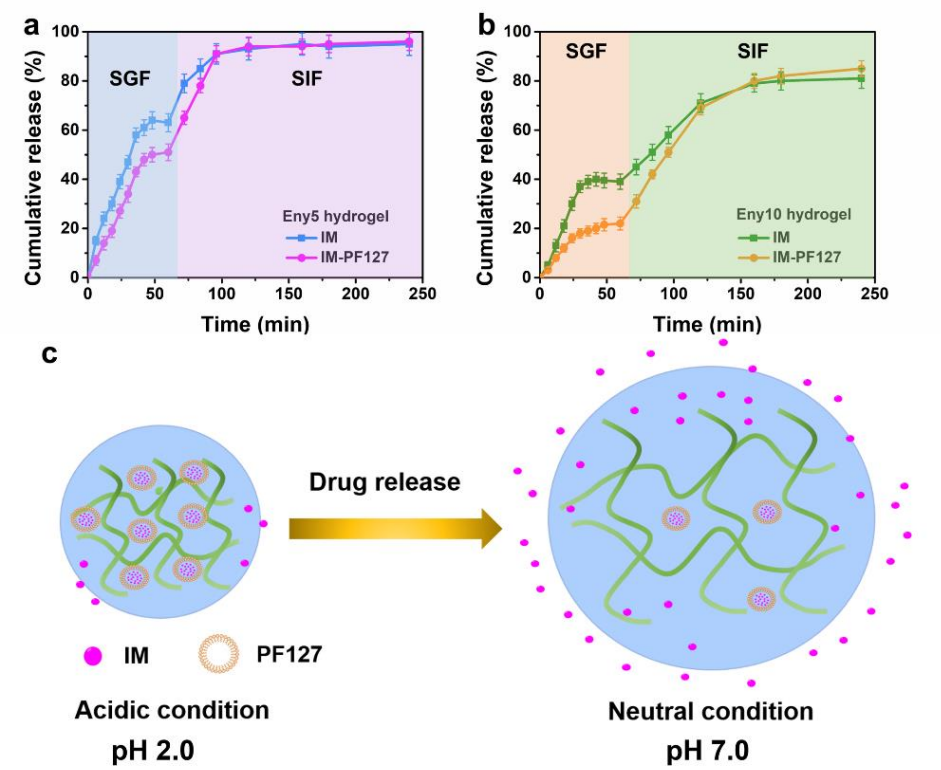

Figure 1-8. *In vitro* release profiles of (a) Eny5 and (b) Eny10 hydrogel loaded with pure IM and IM with PF127 in SGF and SIF. (c) Drug release process under acidic and neutral conditions.

1.4 Conclusion

In this study, the hydrogels were prepared *via* enzymatic crosslinking in the presence of HRP and H_2O_2. The gelation rate and storage modulus of the hydrogels could be tuned by varying the concentrations of HRP and H_2O_2, as well as the DS of PGA-Tyr. The hydrogels formed by PGA-Tyr with a higher DS had a lower swelling ratio and denser pore size. Furthermore, the hydrogels exhibited good reversibility of the pH responsiveness in solutions with different pH values. The biodegradation rate of the hydrogels was related with pH values. Importantly, IM-loaded hydrogels displayed pH-dependent drug release behavior in SGF and SIF. The loading efficiency of IM-micelle-loaded hydrogels with a high DS of PGA-Tyr was markedly enhanced, and the burst release of the drug was markedly depressed in the acidic environment. Therefore, PGA-based hydrogels formed by enzymatic crosslinking have potential applications in oral drug delivery.

References

1. N. Saigal, S. Baboota, A. Ahuja and J. Ali, *Expert Opin. Ther. Pat.*, **2008**, 18, 769–781.
2. F. Ofridam, M. Tarhini, N. Lebaz, É. Gagnière, D. Mangin and A. Elaissari, *Polym. Adv. Technol.*, **2021**, 32, 1455–1484.
3. J. Qu, X. Zhao, P. X. Ma and B. Guo, *Acta Biomater.*, **2018**, 72, 55–69.
4. J. Qu, X. Zhao, P. X. Ma and B. Guo, *Acta Biomater.*, **2017**, 58, 168–180.
5. Y. Liang, X. Zhao, P. X. Ma, B. Guo, Y. Du and X. Han, *J. Colloid Interface Sci.*, **2019**, 536, 224–234.
6. L. Liu, W. Yao, Y. Rao, X. Lu and J. Gao, *Drug Delivery*, **2017**, 24, 569–581.
7. S. Bin Park, M. H. Sung, H. Uyama and D. K. Han, *Prog. Polym. Sci.*, **2021**, 113, 101341.
8. J. Zheng, X. Tian, Y. Sun, D. Lu and W. Yang, *Int. J. Pharm.*, **2013**, 450, 296–303.
9. O. A. Balogun-Agbaje, O. A. Odeniyi and M. A. Odeniyi, *Futur. J. Pharm. Sci.*, **2021**, 7, 1–10.
10. Q. Zhu, W. Song, D. Xia, W. Fan, M. Yu, S. Guo, C. Zhu and Y. Gan, *J. Mater. Chem. B*, **2015**, 3, 8508–8517.
11. B. G. Park, H. Kang, W. Lee, J. S. Kim and T. Son, *J. Appl. Polym. Sci.*, **2013**, 127, 832–836.
12. Z. Yang, Y. Zhang, P. Markland and V. C. Yang, J. Biomed. *Mater. Res. An Off. J.* **2012**, 40 (5), 363−408
13. X. Ma, S. Liu, H. Tang, R. Yang, B. Chi and Z. Ye, *J. Biomater. Sci. Polym. Ed.*, **2018**, 29, 2252–2266.
14. L. S. M. Teixeira, J. Feijen, C. A. van Blitterswijk, P. J. Dijkstra and M. Karperien, *Biomaterials*, **2012**, 33, 1281–1290.
15. M. Khanmohammadi, M. B. Dastjerdi, A. Ai, A. Ahmadi, A. Godarzi, A. Rahimi and J. Ai, *Biomater. Sci.*, **2018**, 6, 1286–1298.
16. M. Kurisawa, J. E. Chung, Y. Y. Yang, S. J. Gao and H. Uyama, *Chem. Commun.*, **2005**, 4312–4314.
17. S. Kobayashi, H. Uyama and S. Kimura, *Chem. Rev.*, **2001**, 101, 3793–3818.
18. H. Uyama and S. Kobayashi, *J. Mol. Catal. B Enzym.*, **2002**, 19–20, 117–127.
19. F. Lee, K. H. Bae and M. Kurisawa, *Biomed. Mater.*, **2015**, 11, 14101.
20. K. Ren, C. He, Y. Cheng, G. Li and X. Chen, *Polym. Chem.*, **2014**, 5, 5069–5076.
21. Q. Xu, C. He, Z. Zhang, K. Ren and X. Chen, *ACS Appl. Mater. Interfaces*, **2016**, 8, 30692–30702.
22. K. Ren, H. Cui, Q. Xu, C. He, G. Li and X. Chen, *Biomacromolecules*, **2016**, 17, 3862–3871.
23. Z. Peng, Y. She and L. Chen, *J. Biomater. Sci. Polym. Ed.*, **2015**, 26, 111–127.
24. Z. Fan, Y. Zhang, W. Zhang and X. Li, J. *Appl. Polym. Sci.* **2015**, 132, 42301.

25. H. Wen, H. Jung and X. Li, *AAPS J.*, **2015**, 17, 1327–1340.
26. M. R. Rekha and C. P. Sharma, *in Peptide and Protein Delivery*, Elsevier, **2011**, pp. 165–194.
27. R. Jin, C. Hiemstra, Z. Zhong and J. Feijen, *Biomaterials*, 2007, 28, 2791–2800.
28. K. M. Park, Y. M. Shin, Y. K. Joung, H. Shin and K. D. Park, *Biomacromolecules*, **2010**, 11, 706–712.
29. K. J. Baynton, J. K. Bewtra, N. Biswas and K. E. Taylor, Biochim. Biophys. *Acta-Protein Struct. Mol. Enzymol.*, **1994**, 1206, 272–278.
30. M. Matsusaki and M. Akashi, *Biomacromolecules*, **2005**, 6, 3351–3356.

Chapter 2.

Preparation of Injectable poly(γ-glutamic acid)-based biodegradable hydrogels with tunable gelation rate and mechanical strength

2.1 Introduction

In recent years, injectable hydrogels have attracted attention for use in tissue regeneration because of their ease of administration, as no invasive surgical or implantation procedures are required, and patient convenience.[1,2] With rapid developments in biomaterial science, research into injectable hydrogels derived from natural or synthetic polypeptides, such as poly(γ-glutamic acid),[3–5] polylysine,[6–8] and poly(L-alanine),[9,10] has increased because of the favorable properties of these hydrogels, such as their excellent biodegradability, biocompatibility, and the extracellular matrix (ECM)-like biomimetic three-dimensional architecture.[11] Poly(γ-glutamic acid) (PGA) is a natto-derived anionic poly(amino acid) formed by an amide linkage between the α-amino group and γ-carboxyl group of two glutamic acid molecules.[3] The large number of carboxylic acid groups in PGA not only offer the ability to introduce functional moieties into PGA precursors, but also can facilitate inter/intramolecular associations by hydrogen bonding and electrostatic interactions with other polymers. Additionally, the amine group in the *N*-terminal γ-glutamic unit can be recognized by γ-glutamyl transpeptidase in the cell membrane, and thus contributes to drug delivery.[12] More recently, much effort has been devoted to designing and developing various PGA-based injectable hydrogels for biomedical applications, especially in tissue engineering scaffolds and drug delivery. Ma et al.[13] modified PGA with hydrazide (PGA-ADH), then combined this with aldehyde hyaluronic acid (HA-CHO) to prepare novel injectable hydrogels. The release of bovine serum albumin (BSA) from these HA/PGA hydrogels showed sustained release behavior (> 30 h). Kim et al.[14] developed injectable PGA-chitosan hydrogels through electrostatic interaction and hydrophobic association,

and the hydrogel formed *in vivo* showed long term (~2 weeks) stability without noticeable inflammatory response. Sun et al.[15] used glycidyl methacrylate (GMA) to modify polylysine and PGA to prepare an injectable polypeptide-based hydrogel through photopolymerization. This hydrogel showed a wide spectrum of antibacterial activity and promoted wound healing. Yang et al.[16] fabricated injectable PGA hydrogels, based on methacrylate-PGA and cysteamine-functionalized PGA, via thiol-Michael addition reactions for cartilage regeneration. Notably, PGA modified with different functional groups was used to prepare hydrogels, PGA-based hydrogels still showed good cytocompatibility,[16-19] which may be related to the intrinsic excellent biocompatibility of the PGA backbone. Nevertheless, the main obstacle in the development of PGA-based hydrogels is that it is difficult to achieve satisfactory mechanical properties and rapid injection time simultaneously, which greatly limits their application for load-bearing tissue engineering.

Currently, various strategies, such as combining different physical or chemical crosslinking methods[18,20,21] and constructing hybrid hydrogels[22,23] have been employed to meet the required toughness and injection time for PGA-based hydrogels for specific biomaterial applications. For instance, Chi et al.[18] fabricated novel dual crosslinking injectable PGA-based hydrogels though a thiol-ene click reaction and hydrogen-bond interaction between DL-1,4-dithiothreitol and GMA-modified PGA. The formed hydrogel had advantages for use in cartilage repair because it had a short gelation time and good toughness. Furthermore, this group also incorporated hyaluronic acid (HA) in PGA-based hydrogels to construct interpenetrating polymeric network HA/PGA adaptable hydrogels with injectability and a fast shape recovery capacity.[20] Among the preparation approaches for injectable hydrogels, enzymatic crosslinking is a good choice for the development of *in situ* formed hydrogels because of the rapid gelation time, tunable mechanical properties, mild reaction conditions, and non-toxic nature.[24-26] Previously, our group has prepared injectable biodegradable hydrogels composed of HA-tyramine conjugates via enzymatic crosslinking. The gelation time and mechanical properties of this hydrogel could be easily controlled by changing the horseradish

peroxidase (HRP) and hydrogen peroxide (H_2O_2) concentrations.[24] Peng et al.[27] have synthesized an *in situ*-formed hydrogel by the enzymatic crosslinking of poly(γ-glutamic acid)-tyramine conjugates for the controlled release of proteins. Ren et al.[28] have developed an injectable hydrogel comprising poly(L-glutamic acid)-graft-tyramine through enzymatic crosslinking, and this hydrogel could regulate the cellular microenvironment. The Diels-Alder (DA) reaction has high selectivity, no need for a catalyst and no by-products.[29,30] Hydrogels formed by the DA reaction have been widely used in cartilage tissue repair, because they exhibit a uniform network structure, good mechanical properties and biocompatibility.[31-33] However, to the best of our knowledge, a PGA hydrogel fabricated by the integration of enzymatic crosslinking and DA reactions has not been reported yet. Thus, we attempted to design and prepare a versatile PGA hydrogel with a rapid gelation rate and excellent toughness for application in tissue engineering scaffolds.

In this study, inspired by natural protein-based ECM, we designed a versatile dual cross-linking PGA hydrogel with rapid injectability and controllable mechanical properties. The dual crosslinking hydrogels (DA-Eny hydrogels) were synthesized using furfurylamine and tyramine-modified PGA (PGA-Fa-Tyr) and dimaleimide poly(ethylene glycol) (MAL-PEG-MAL) via combining enzymatic crosslinking and DA reaction in a mild manner. The enzymatic crosslinking method endowed the hydrogels with a fast gelation rate and tunable mechanical strength, and excellent toughness was achieved by the creation of an enhanced network through the DA reaction. The rheological behavior and compressive mechanical properties of the DA-Eny hydrogels were tested by rheometer. The morphology of DA-Eny hydrogels was characterized by scanning electron microscopy (SEM). The physicochemical properties of the DA-Eny hydrogels, such as the gelation time, swelling ratio and degradation behavior, were also studied in detail. In addition, the DA-Eny hydrogels encapsulating BSA were also investigated *in vitro*. This investigation extends the application of polypeptide-based hydrogels in biomedical fields, such as tissue engineering and cell/drug delivery.

2.2 Experimental

Materials

Poly(γ-glutamic acid) (PGA, M_w = 1.6× 10^5 g/mol) (Seoul, Korea). Tyramine hydrochloride (Tyr), furfurylamine (Fa), 4-(4,6-dimethoxy-1,3,5-triazin-2-yl)-4-methylmorpholinium chloride (DMTMM), Dimaleimide poly(ethylene glycol) (MAL-PEG-MAL) (M_w = 6 × 10^3 g/mol) was purchased from PolyScience (PA, USA). 2-morpholinoethanesulfonic acid (MES), proteinase K and bovine serum albumin (BSA) were purchased from Sigma-Aldrich (St. Louis, USA).

Synthesis of PGA-Fa-Tyr

PGA (1.35 g, 10.0 mmol carboxyl groups) was dissolved in 135 mL of MES buffer (0.1 mol/L, pH 5.5). Subsequently, the carboxyl groups were activated by adding DMTMM (2.21 g, 8.0 mmol) for 10 min. Furfurylamine (300 μL, 6.7 mmol) was then added dropwise, the mixture was stirred at 30 °C for 24 h. Then, the remaining non-activated carboxyl groups were activated by adding DMTMM (2.77 g, 10.0 mmol) for another 10 min. Then, tyramine hydrochloride (1.38 g, 8.0 mmol) was added, and the mixture was stirred for another 24 h at 30 °C. The solution was dialyzed against deionized water for 3 d using a dialysis membrane with a molecular weight cut-off (MWCO) of 1×10^4. A white spongy product PGA-Fa-Tyr was obtained by lyophilization (**Scheme 2-1**).

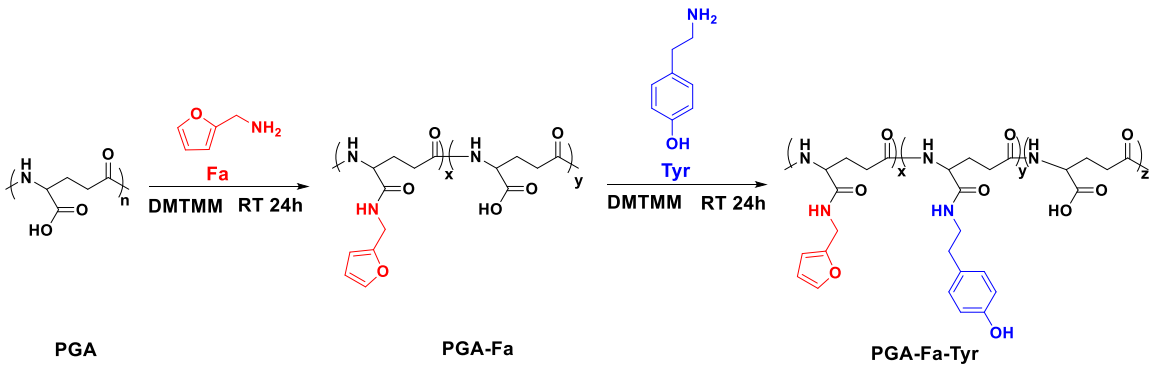

Scheme 2-1. Synthesis of PGA–Fa-Tyr.

Hydrogel formation and injectability

The vial inverting method was used to measure the gelation time of the hydrogels.[24] The synthetic route of the hydrogels is shown in **Scheme 2-2**. PGA-Fa-Tyr (70 mg) was dissolved in 1.95 mL of PBS (pH 7.4) in a vial. Then MAL-PEG-MAL (molar ratios of furan: maleimide = 5.0 and 1.0) was added into the solution. Freshly prepared HRP (25 μL, 2.5 U/mL) and H_2O_2 solutions (molar ratios of H_2O_2: Tyr = 0.05, 0.10, 0.25, 0.40, and 0.50) were added into the vial and gently vortexed. When no fluidity was visually observed upon inverting the vial, the gel state was determined. The hydrogels were formed through the enzymatic crosslinking process. Then, the hydrogels were placed into a bio-shaker to incubate for 12 h at 37 °C and the DA reaction, as the second crosslinking reaction, occurred during this period. The final concentration of PGA-Fa-Tyr was 3.5% (w/v). Hydrogels formed by dual cross-linking were named as DA*x*-*y*-Eny*z* hydrogel, hydrogels formed by single cross-linking were named as DA*x*-*y* and Eny*z* hydrogel (*x*-*y* represents the molar ratio of furan/maleimide, *z* represents the molar ratio of H_2O_2/Tyr).

To investigate the injectability of the hydrogel, an orange dye was mixed with the prepared precursors of the hydrogel and drawn into 20-gauge double syringe.

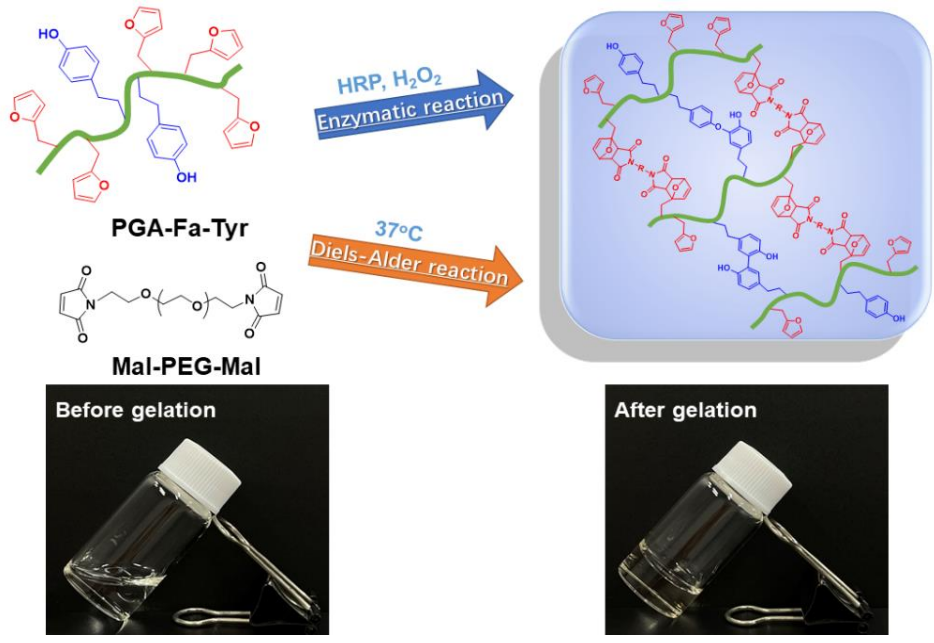

Scheme 2-2. Schematic diagram of the formation of the hydrogels.

Characterization

A lyophilized PGA-Fa-Tyr sample was characterized by ^{1}H-NMR (Bruker AVANCE 400 MHz, Germany) with D_2O as the solvent. Attenuated total reflection Fourier transform infrared (ATR-FTIR) spectroscopy (Thermo Scientific Nicolet iS 5, USA) was used to confirm the presence of the -C=C-in the Diels-Alder adduct. The samples for FTIR spectroscopy were swollen in PBS to remove the unreacted reagents, then frozen with liquid nitrogen and dried in a vacuum freeze drier for ATR-FTIR measurement. Morphologies of the hydrogels were characterized using scanning electron microscopy (Hitachi SU3500, Japan). The hydrogel samples were freeze-dried and sputtered with gold by using an MSP-1S magnetron sputter (Vacuum Device Inc, Japan). The samples were observed under high vacuum at an accelerating voltage of 1.50 kV.

Mechanical properties of hydrogels

The rheological analyses of the hydrogels were performed with a Hakke Rheostress 6000 (Thermo Scientific, USA) equipped with 20-mm diameter parallel plates. PGA-Fa-Tyr, MAL-PEG-MAL, and HRP solutions were mixed homogeneously and loaded onto the bottom plate, and the upper plate was lowered to a gap size of 1.0 mm. A solution of H_2O_2 at different concentrations was immediately added to the mixture. To observe the change of storage modulus (G') and loss modulus (G'') during the first enzymatic crosslinking and second DA crosslinking, oscillation time sweep was carried out at 20 °C under 0.1% strain and 1 Hz, then the temperature was increased to 37 °C after the modulus values reached a plateau. The oscillation frequency sweep was conducted from 0.1 to 10 Hz at 0.1% strain and 37 °C to determine the G' value of the hydrogels. Silicon oil was used to trap the mixture to prevent the evaporation of water during the test. The axial ramp test was used to obtain the compression stress-strain curve. The prepared cylindrical hydrogel (diameter 13.0 mm, height 5.0 mm) was loaded to the bottom plate at 0.5 mm/s at 25 °C. The compression modulus (E) was calculated as the slope of the stress-strain curve, in the range of strain from 15% to 20%. The rheological and compression experiments were performed in triplicate.

Swelling ratio of hydrogels

Eny-DA hydrogels and control hydrogels were accurately weighed (W_0) and immersed in 10 mL of PBS (pH 7.4) at 37 °C. After 48 h, the hydrogels reached swelling equilibrium. The swollen samples were taken out from the PBS after removing the water on the surface and weighed immediately (W_1). The swelling ratio of the hydrogels was calculated using the following equation (**equation 2.1**):

$$Swelling\ ratio = \frac{W_1 - W_0}{W_0} \times 100\% \quad (2.1)$$

The swelling ratios were measured in triplicate and the values were averaged.

***In vitro* degradation of hydrogel**

For the degradation test, hydrogel samples were lyophilized and weighed (W_{l1}), then the samples were submerged in fresh pH 7.4 PBS buffer with and without proteinase K (10 U/mL). At selected time points, the samples were removed and lyophilized again to obtain the dried mass (W_{l2}). The proteinase K solution was replaced in each sample at each time point with a fresh solution. The remaining mass of the hydrogels was defined by the following equation (**equation 2.2**):

$$Remaining\ mass = \frac{W_{l2}}{W_{l1}} \times 100\% \quad (2.2)$$

The degradation experiments were performed in triplicate and the values were averaged.

Protein encapsulation and *in vitro* release

BSA as a model drug was encapsulated into the hydrogels to investigate the *in vitro* release. First, PGA-Fa-Tyr (70 mg), MAL-PEG-MAL, and BSA (1.0 mg/mL) were dissolved in 1.95 mL of PBS, and HRP and H_2O_2 solutions were added to form hydrogels. Then, the hydrogels were transferred into a bio-shaker for 12 h at 37 °C for the DA reaction to completely occur. The BSA-loaded samples were subsequently incubated in 10 mL of PBS solution (pH 7.4) at 37 °C. At various times, 2.0 mL of the incubated solution was taken out and replaced with an equal volume of fresh PBS solution. The concentration of BSA was quantified by microplate spectrophotometer

(Synergy HT SIAFR-4, USA) at 280 nm. The release experiments were performed in triplicate.

2.3 Results and discussion

Characterization of PGA-Fa-Tyr and hydrogels

PGA-Fa-Tyr was prepared in a two-step reaction by modification of PGA with furfurylamine and tyramine hydrochloride with DMTMM regent. In **Figure 2-1**, the characteristic peaks of furan and tyramine can be seen in the ^{1}H-NMR spectra. The characteristic peaks of the furan group appear at 6.09, 6.20, and 7.25 ppm, and the peaks of the phenol group appear at 6.61 and 6.91 ppm. The degree of substitution (DS) was calculated by comparing the integral areas of the furan group and the phenol group with the area of the proton peak assigned to the methylene in the glutamate unit (-CH_2CH_2CO-) at approximately 1.65-2.18 ppm. The DS of PGA-Fa and PGA-Tyr was approximately 37.6% and 6.4%, respectively. The ^{1}H-NMR spectra indicated the successful grafting of furan and phenol groups onto the PGA backbone.

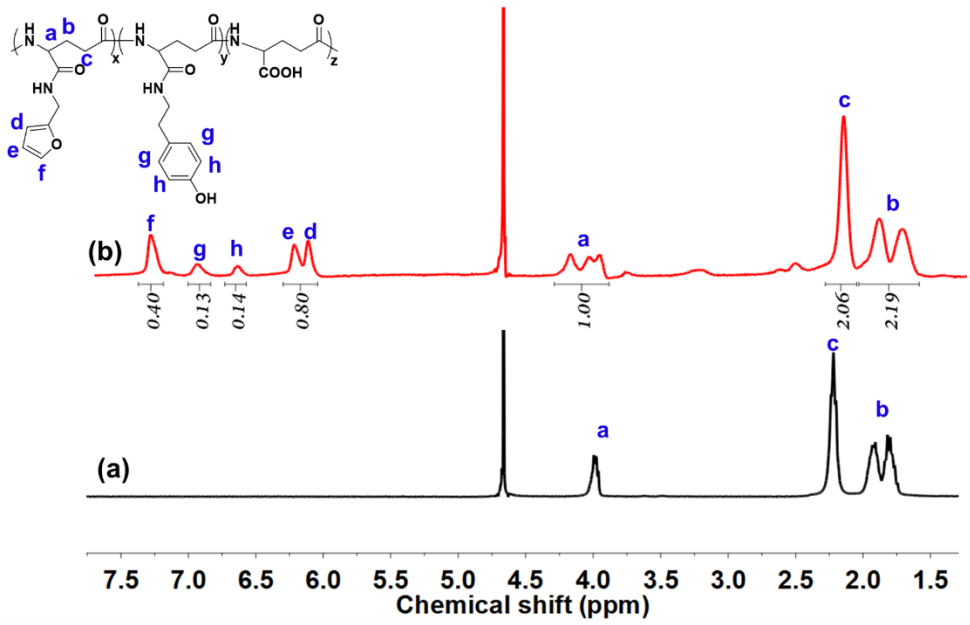

Figure 2-1. ^{1}HNMR spectra of PGA (a) and PGA-Fa-Tyr (b) in D_2O.

FTIR characterization was employed to confirm the formation of the DA adduct of the DA-Eny Hydrogel. **Figure 2-2** shows the FTIR spectra of PGA, PGA-Fa-Tyr, Mal-

PEG-Mal, and the DA1-1-Eny0.5 hydrogel. The peaks in the spectra of PGA-Fa-Tyr and Mal-PEG-Mal at 1532 and 1466 cm^{-1} correspond to the C=C group of the furan in PGA-furan and the maleimide in Mal-PEG-Mal, respectively. Alkene bending was also quite distinct in the Mal-PEG-Mal spectrum with a sharp signal at 695 cm^{-1}, corresponding to the C=C of the maleimide. In the DA-Eny hydrogel spectrum, these C=C signals had disappeared with the appearance of an absorption at 1452 cm^{-1} (C=C in the adduct), implying the removal of individual furan and maleimide groups and the generation of a maleimide-furan cycloaddition product during the DA reaction.

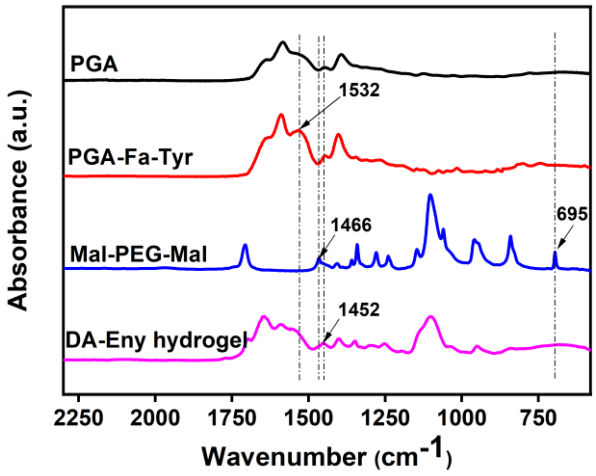

Figure 2-2. FTIR spectra of PGA, PGA-Fa-Tyr, Mal-PEG-Mal, and DA adduct.

Gelation time and injectability of hydrogels

The gelation time of the DA-Eny hydrogels relied on the rapid enzymatic crosslinking. **Figure 2-3a** shows the gelation times of the DA-Eny hydrogels using different concentrations of HRP and H_2O_2, which were assessed by the vial inverting method. When H_2O_2/Tyr ratio was 0.05, the gelation time significantly decreased from 280 to 55 s as the concentration of HRP increased from 1.0 to 5.0 U/mL, which was attributed to the higher enzyme activity. In addition, the gelation time gradually decreased when the H_2O_2/Tyr molar ratio was increased from 0.05 to 0.50. Thus, the gelation time could be controlled by varying the concentrations of H_2O_2 and HRP. Considering the practical applications of injectable hydrogels, an appropriate gelation rate is very necessary. Fast gelation behavior would tend to block needles during

injection, whereas a slow gelation process may cause the hydrogel precursors encapsulating drugs or cells to diffuse away from the target sites. Therefore, 2.5 U/mL HRP was chosen to prepare injectable hydrogels with a satisfactory gelation time ranging from approximately 95 to 10 s. It is essential that injectable hydrogels used in bioengineering can be injected into irregular sites to form the gel *in situ* to achieve the structural and functional restoration of damaged tissues. Owing to the rapid gelation based on enzymatic crosslinking, the extruded polymer solutions assembled to form an integral hydrogel. DA-Eny hydrogel precursors injected into a Petri dish using a 20-gauge double syringe could form different shapes. The letters "O" and "U" were successfully written as shown in **Figure 2-3b**.

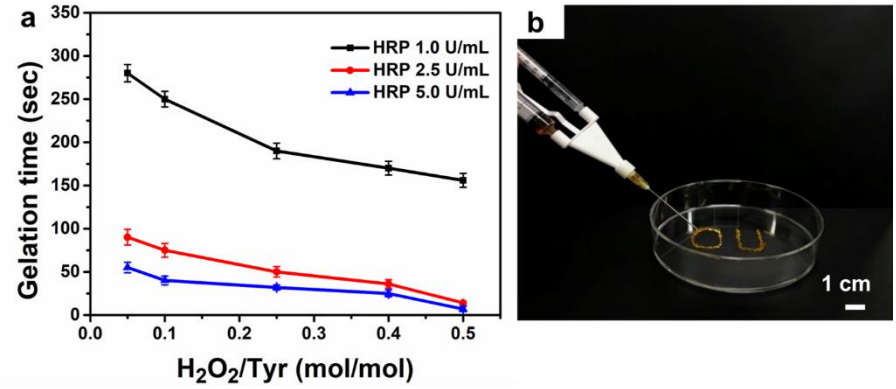

Figure 2-3 (a) Dependence of gelation time on the concentrations of HRP and H_2O_2. (b) Photograph of the injectability of the hydrogel (HRP=2.5 U/mL, H_2O_2/Tyr = 0.05).

Rheological behavior of DA-Eny hydrogels

The viscoelastic characteristics of the injectable DA-Eny hydrogels were measured by monitoring the variations in G' and G'' values against time and temperature. As shown in **Figure 2-4**, the values of G' and G'' increased with time, however, the value for G' increased faster than for G'' and finally exceeded G''. As expected, rapid gelation was observed for the DA5-1-Eny0.05 and DA1-1-Eny0.05 hydrogels because of the enzymatic crosslinking. The gelation times were approximately 90 and 92 s for the DA5-1-Eny0.05 and DA1-1-Eny0.05 hydrogels, respectively, which were close to the gelation time measured by the vial inverting method. When the temperature was increased to 37 °C, the storage modulus steeply increased and reached a plateau over

time after the enzymatic crosslinking had finished. Additionally, the value of G' for the DA1-1-Eny0.05 hydrogels reached a plateau faster than that of DA5-1-Eny0.05 and the maximum G′ value of the DA1-1-Eny0.05 hydrogels was an order of magnitude greater than that of DA5-1-Eny0.05. These results indicated that higher temperatures could effectively stimulate the DA reaction as the second crosslinking reaction in the hydrogel. Furthermore, FTIR characterization confirmed the generation of a maleimide-furan cycloaddition product in the hydrogel. Consequently, it appears that the DA reaction took place inside of the DA-Eny hydrogels as the temperature increased, ultimately resulting in storage and loss modulus enhancement of the hydrogels.

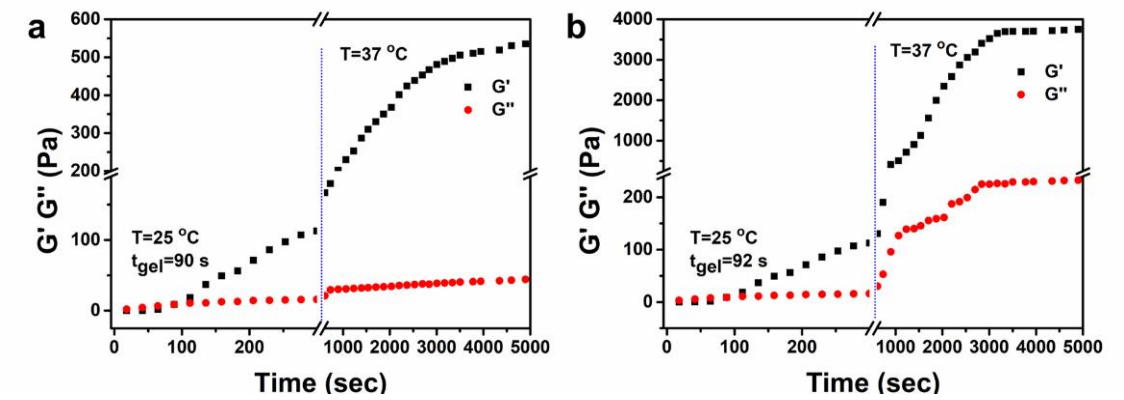

Figure 2-4. The storage modulus (G') and loss modulus (G'') of the DA5-1-Eny0.05 hydrogel (a) and DA1-1-Eny0.05 hydrogel (b) as a function of time.

To further investigate the reinforcing effect of the second DA network on the Eny hydrogels, the G' values of the hydrogels were measured as shown in **Figure 2-5**. The G' values of the Eny and DA hydrogels increased with increasing H_2O_2/Tyr ratios and increasing molar ratios of furan/maleimide, respectively. After integrating the enzymatic crosslinking with the DA reaction to prepare the DA-Eny hydrogels, the dual crosslinking hydrogels showed an apparently higher storage modulus than that of the Eny hydrogels. For instance, the storage modulus of the DA5-1-Eny hydrogels was approximately 1.5-4.0-fold higher than that of Eny hydrogels. Moreover, when the molar ratio of furan/maleimide was 1:1, the corresponding G' values of the DA1-1-Eny hydrogels were closer to, but still larger than, the values of the DA hydrogels, because the increased crosslinking density leads to a tighter structure for the DA1-1-Eny

hydrogels. These results indicated that using the DA reaction for a second crosslinking in the hydrogel was an efficient way to enhance the storage modulus of the Eny hydrogels. Furthermore, the *G′* values were related to the gelation time: the shorter the gelation time, the higher the G′ value, which was in agreement with the results previously reported by our group. As shown in **Figure 2-5**, the storage modulus values of the DA5-1-Eny hydrogels (520-3390 Pa) and DA1-1-Eny hydrogels (3700-6980 Pa) were similar to those of brain and nerve tissues (100-1000 Pa) and liver, relaxed muscle, and breast gland tissue (1000-10000 Pa)[34] indicating these gels have potential as tissue engineering scaffolds for encapsulating different cell types.

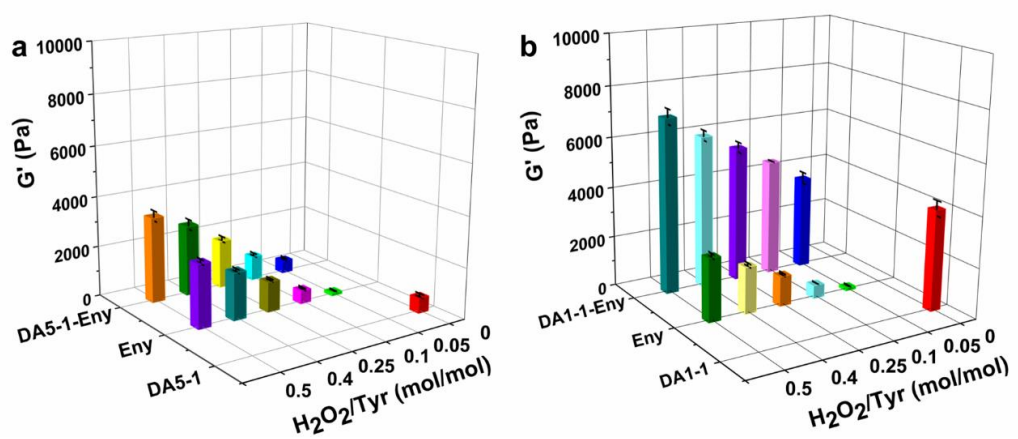

Figure 2-5. The storage modulus of DA hydrogels, Eny hydrogels, and DA-Eny hydrogels.

Mechanical properties of hydrogels

The mechanical properties of the hydrogels were evaluated by a compression test. As shown in **Figure 2-6a**, the compressive strain of the Eny hydrogels decreased in spite of an increase in the compressive strength with increasing H_2O_2/Tyr ratios. When the H_2O_2/Tyr ratio was 0.50, the Eny hydrogel had the highest compressive stress (20.0 kPa) but the lowest compressive strain (43.7%). Whereas the DA1-1 hydrogel with a compressive stress of 74.4 kPa and compressive strain of 79.5% was stronger and more flexible than the Eny hydrogels. In particular, the compressive stress and strain of the DA-Eny hydrogels were superior to the Eny hydrogels, the compressive stress and strain of the DA1-1-Eny0.5 hydrogel were approximately 7.0- and 1.5-fold higher, respectively, compared with the Eny0.5 hydrogel. When the H_2O_2/Tyr ratio was same,

with increasing molar ratios of furan/maleimide, the DA1-1-Eny hydrogels showed greater compressive strength and fracture strain than the DA5-1-Eny hydrogels (**Figure 2-6 b,c**). As shown in **Figure 2-7**, when the compressive strain was 50%, the Eny0.5 hydrogel was easily broken, while the DA1-1-Eny0.5 hydrogel maintained structural integrity after release. The structural integrity was maintained because, through introducing DA crosslinking, the DA1-1-Eny0.5 hydrogel had a high content of DA adducts, resulting in an anti-compressive network. These results indicated that the DA adduct content had a considerable impact on the mechanical properties of the hydrogels. However, with increasing H_2O_2/Tyr ratios, both the DA5-1-Eny hydrogels and DA1-1-Eny hydrogels displayed a trend toward a reduction in the fracture strain, which was attributed to the inherent features of enzymatic cross-linking. In addition, it can be seen in **Figure 2-6d** that the compressive modulus values of the DA1-1-Eny hydrogels were approximately 2.0-3.5-fold higher than those of the DA5-1-Eny hydrogels, because of the high amount of DA adducts in the DA1-1-Eny hydrogels, leading to a tighter structure. These results indicated that the greater the molar ratio of furan/maleimide, the stronger the toughening effect on the DA-Eny hydrogels.

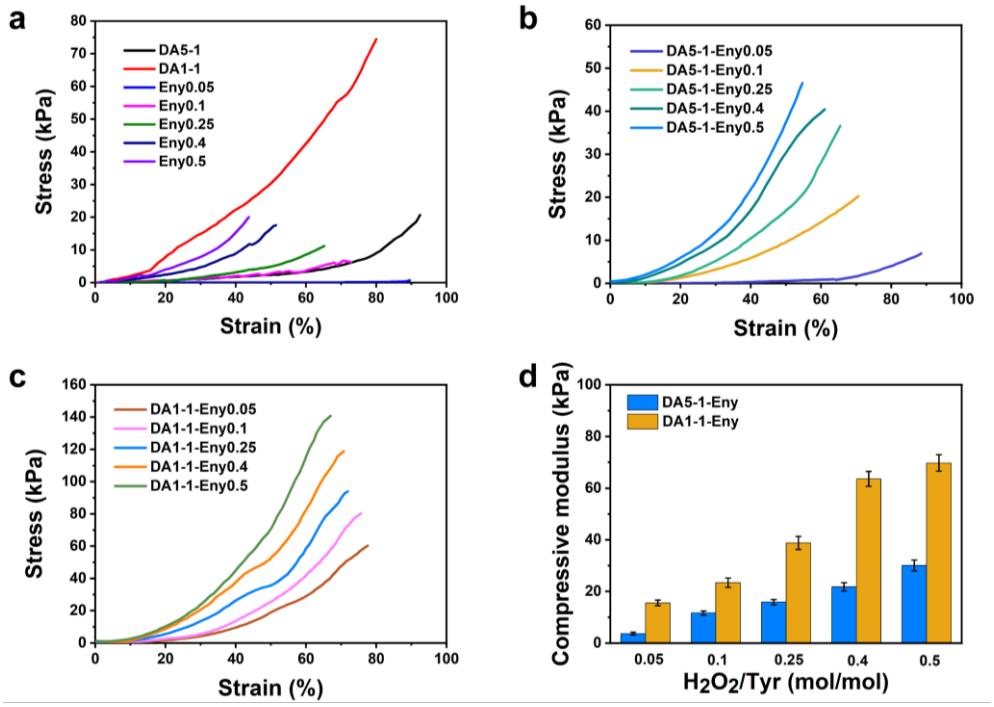

Figure 2-6. Compression stress-strain curves of (a) control hydrogels, (b) DA5-1-Eny hydrogels, and (c) DA1-1-Eny hydrogels. (d) compressive modulus of DA-Eny hydrogels.

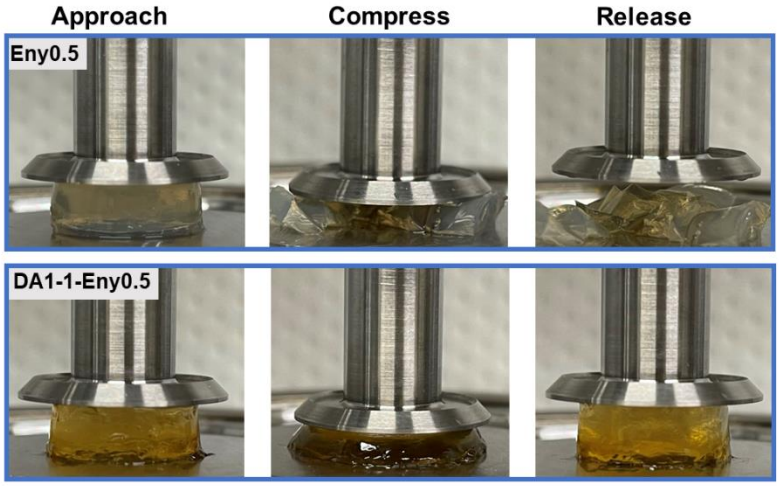

Figure 2-7. Images of the compression and release processes of hydrogels under 50% deformation.

Swelling ratio, morphology and *in vitro* degradation of DA-Eny hydrogels

The equilibrium swelling ratios of the DA-Eny hydrogels are shown in **Figure 2-8a**. The swelling ratios of the DA1-1-Eny hydrogels were remarkably lower than those of the DA5-1-Eny hydrogels, which was attributed to the higher proportion of DA adducts in the DA1-1-Eny hydrogels, resulting in a denser network. In addition, with increasing H_2O_2/Tyr ratios from 0.05 to 0.50, the swelling ratios of the DA5-1-Eny hydrogels and DA1-1-Eny hydrogels showed a tendency to decrease. These results suggest that the swelling ratios of the DA-Eny hydrogels could be adjusted by changing the molar ratios of furan/maleimide or H_2O_2/Tyr.

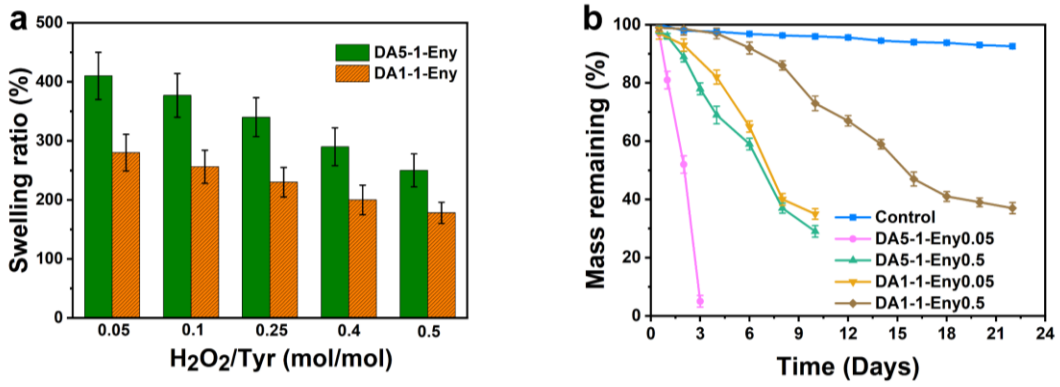

Figure 2-8. (a) Swelling ratio of DA-Eny hydrogels in pH 7.4 PBS. (b) Mass degradation percentage of DA-Eny hydrogels in pH 7.4 PBS.

The pore size and pore interconnectivity are critical factors for the hydrogels applied in tissue engineering. Because they can provide the supply of nutrients and the removal of waste products, as well as affect the attachment, migration and proliferation of cells. The lyophilized DA-Eny hydrogels showed interconnected porous structures as shown in **Figure 2-9**. DA1-1-Eny hydrogel displayed a more compact network structure compared with the DA5-1-Eny hydrogel, which was attributed to high content of DA adducts in the DA1-1-Eny hydrogels. Furthermore, the decrease of pore size with increasing H_2O_2/Tyr ratios from 0.05 to 0.50 was due to an enhancement in the degree of crosslinking in the hydrogel. The swelling ratio was closely related to the pore size of the hydrogels, the denser pore size of the hydrogel, the lower swelling ratio of the hydrogel.

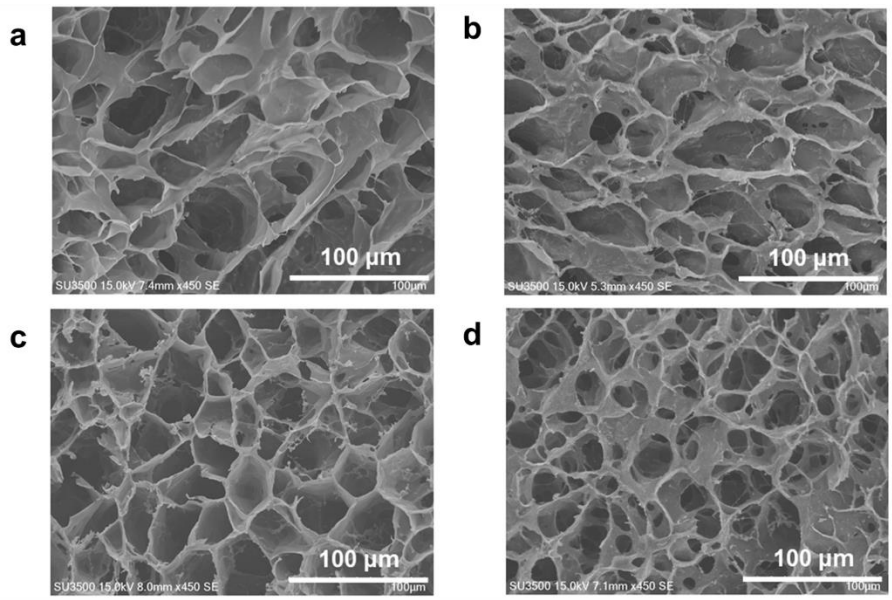

Figure 2-9. SEM images of the lyophilized (a) DA5-1-Eny0.05 hydrogel, (b) DA5-1-Eny0.5 hydrogel, (c) DA1-1-Eny0.05 hydrogel, and (d) DA1-1-Eny0.5 hydrogel.

Appropriate biodegradation properties are essential for injectable hydrogels used for tissue regeneration. The degradation behavior of the DA-Eny hydrogels was assessed by incubating the hydrogels in pH 7.4 PBS buffer solutions with and without proteinase K as shown in **Figure 2-8b**. The DA5-1-Eny0.05 hydrogel showed complete degradation in 3 days via the cleavage of the polypeptide chains in the presence of proteinase K, whereas the DA5-1-Eny0.05 hydrogel without proteinase K kept its

integrity for up to 22 days under the same conditions. Moreover, the DA1-1-Eny0.05 hydrogel degraded slowly with 97% mass remaining after 3 days compared with the DA5-1-Eny0.05 hydrogel. This result was ascribed to the fact that the DA1-1-Eny hydrogels with a higher molar ratio of furan/maleimide had a higher crosslinking density. Furthermore, the degradation rate of the DA1-1-Eny0.5 hydrogel was obviously lower than that of the DA1-1-Eny0.05 hydrogel, which was because of the increase in the H_2O_2/Tyr ratio, leading to an increase in the degree of crosslinking in the hydrogel. This is consistent with the porous structure of hydrogels in **Figure 2-9**, the looser porous structure will contribute to faster degradation behavior. These results demonstrated that the degradation behavior of the DA-Eny hydrogels was affected by the degree of crosslinking of the hydrogels. It is worth noting that the degradation products of PGA have no cytotoxicity.[35] Hence, we could regulate the degradation behavior of the DA-Eny hydrogels by adjusting the H_2O_2/Tyr and furan/maleimide ratios.

***In vitro* protein release**

The controlled-release delivery of proteins is an important method to make cell growth factor maintain biologically active *in vivo*. Therefore, achieving long-term release of proteins is valuable and beneficial for cell growth. Here, BSA was used as a model protein to study the release behavior. As depicted in **Figure 2-10**, the DA hydrogels and the Eny hydrogels prepared with a single crosslinking showed a burst release (approximately 46%-95%) within 12 h, whereas the release of BSA from the DA-Eny hydrogels except for DA5-1-Eny0.05 was less than 29% in 12 h. Compared with the DA5-1-Eny hydrogels, the release of BSA from the DA1-1-Eny hydrogels exhibited a decreasing trend for the same H_2O_2/Tyr ratio. When the furan/maleimide ratio was the same, the release rate of BSA from the DA-Eny hydrogels also gradually decreased with increasing H_2O_2/Tyr ratios. These results suggested that the release behavior of BSA from the DA-Eny hydrogels was affected by the crosslinking density. In addition, all the DA-Eny hydrogels, except for DA5-1-Eny0.05, exhibited a sustained release effect with a long duration (120 h, 63%-72% BSA release). Overall,

the release of BSA encapsulated in DA-Eny hydrogels showed an obvious sustained release behavior (>70 h), which is meaningful for protein and drug delivery.

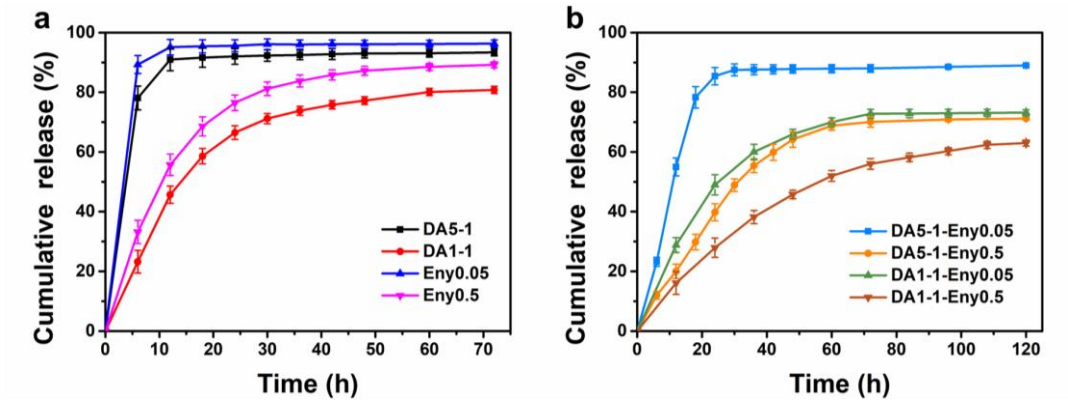

Figure 2-10. *In vitro* release profiles of BSA from DA hydrogels and Eny hydrogels (a) and DA-Eny hydrogels (b) in pH 7.4 PBS.

2.4 Conclusions

In this study, injectable PGA hydrogels were prepared by integrating enzymatic crosslinking with DA reaction. The DA-Eny hydrogels had a rapid gelation time (within 95 s). After introducing the DA reaction, the storage modulus, mechanical strength, and anti-compression ability of the DA-Eny hydrogels were improved, indicating that incorporating the DA reaction has an outstanding toughening effect on DA-Eny hydrogels. The equilibrium swelling, pore size and degradation rates could be adjusted by changing the molar ratios of furan/maleimide and H_2O_2/Tyr. Furthermore, BSA-loaded DA-Eny hydrogels exhibited sustained release behavior in a controllable fashion. Therefore, these injectable DA-Eny hydrogels formed by a controllable and straightforward approach have potential applications in tissue engineering scaffolds and drug delivery.

References

1. Y. Li, J. Rodrigues and H. Tomás, *Chem. Soc. Rev.*, **2012**, 41, 2193–2221.
2. K. H. Bae, L. S. Wang and M. Kurisawa, *J. Mater. Chem. B*, **2013**, 1, 5371–5388.
3. S. Bin Park, M. H. Sung, H. Uyama and D. K. Han, *Prog. Polym. Sci.*, **2021**, 113, 101341.
4. M. H. Kim, J. N. Lee, J. Lee, H. Lee and W. H. Park, *ACS Biomater. Sci. Eng.*, **2020**, 6, 3103–3113.
5. S. Yan, T. Wang, L. Feng, J. Zhu, K. Zhang, X. Chen, L. Cui and J. Yin, *Biomacromolecules*, **2014**, 15, 4495–4508.
6. S. Liu, X. Liu, Y. Ren, P. Wang, Y. Pu, R. Yang, X. Wang, X. Tan, Z. Ye, V. Maurizot and B. Chi, *ACS Appl. Mater. Interfaces*, **2020**, 12, 27876–27888.
7. Y. Wang, H. Cao and X. Wang, *Mater. Chem. Phys.*, **2020**, 248, 122902.
8. S. C. Shukla, A. Singh, A. K. Pandey and A. Mishra, *Biochem. Eng. J.*, **2012**, 65, 70–81.
9. E. J. Yun, B. Yon, M. K. Joo and B. Jeong, *Biomacromolecules*, **2012**, 13, 1106–1111.
10. J. H. Hong, H. J. Lee and B. Jeong, *ACS Appl. Mater. Interfaces*, **2017**, 9, 11568–11576.
11. C. He, X. Zhuang, Z. Tang, H. Tian and X. Chen, *Adv. Healthc. Mater.*, **2012**, 1, 48–78.
12. Z. X. Liao, S. F. Peng, Y. L. Chiu, C. W. Hsiao, H. Y. Liu, W. H. Lim, H. M. Lu and H. W. Sung, *J. Control. Release*, **2014**, 193, 304–315.
13. X. Ma, T. Xu, W. Chen, H. Qin, B. Chi and Z. Ye, *Carbohydr. Polym.*, 2**018**, 179, 100–109.
14. W. Kim, M. Kim and G. Tae, *Int. J. Biol. Macromol.*, **2018**, 110, 457–464.
15. Sun, X. He, L. Li, T. Li, Q. Liu, X. Zhou, X. Ji, W. Li and Z. Qian, *NPG Asia Mater.*, **2020**, 12, 1–11.
16. R. Yang, X. Wang, S. Liu, W. Zhang, P. Wang, X. Liu, Y. Ren, X. Tan and B. Chi, *Int. J. Biol. Macromol.*, **2020**, 142, 332–344.
17. W. Chen, R. Wang, T. Xu, X. Ma, Z. Yao, B. Chi and H. Xu, *J. Mater. Chem. B*, **2017**, 5, 5668–5678.
18. S. Liu, Y. Pu, R. Yang, X. Liu, P. Wang, X. Wang, Y. Ren, X. Tan, Z. Ye and B. Chi, *Int. J. Biol. Macromol.*, **2020**, 153, 158–168.
19. M. I. Bajestani, S. Kader, M. Monavarian, S. M. Mousavi, E. Jabbari and A. Jafari, *Int. J. Biol. Macromol.*, **2020**, 142, 790–802.
20. X. Ma, X. Liu, P. Wang, X. Wang, R. Yang, S. Liu, Z. Ye and B. Chi, *ACS Appl. Bio Mater.*, **2020**, 3, 4036–4043.
21. P. Wang, W. Zhang, R. Yang, S. Liu, Y. Ren, X. Liu, X. Tan and B. Chi, *Int. J. Biol. Macromol.*, **2021**, 167, 1508–1516.
22. Q. Gao, C. Zhang, M. Wang, Y. Wu, C. Gao and P. Zhu, *Polymer.*, **2020**, 197, 122489.
23. C. Dou, Z. Li, J. Gong, Q. Li, C. Qiao and J. Zhang, *Int. J. Biol. Macromol.*, **2021**, 170, 354–365.
24. M. Kurisawa, J. E. Chung, Y. Y. Yang, S. J. Gao and H. Uyama, *Chem. Commun.*, **2005**, 4312–4314.
25. R. Jin, L. S. Moreira Teixeira, P. J. Dijkstra, C. A. van Blitterswijk, M. Karperien and J.

Feijen, *Biomaterials*, **2010**, 31, 3103–3113.
26. F. Lee, J. E. Chung and M. Kurisawa, *Soft Matter*, **2008**, 4, 880–887.
27. Z. Peng, Y. She and L. Chen, *J. Biomater. Sci. Polym. Ed.*, **2015**, 26, 111–127.
28. K. Ren, H. Cui, Q. Xu, C. He, G. Li and X. Chen, *Biomacromolecules*, **2016**, 17, 3862–3871.
29. M. Juhl and D. Tanner, *Chem. Soc. Rev.*, **2009**, 38, 2983–2992.
30. K. C. Koehler, K. S. Anseth and C. N. Bowman, *Biomacromolecules*, **2013**, 14, 538–547.
31. F. Yu, X. Cao, Y. Li, L. Zeng, B. Yuan and X. Chen, *Polym. Chem.*, **2014**, 5, 1082–1090.
32. F. Yu, X. Cao, J. Du, G. Wang and X. Chen, *ACS Appl. Mater. Interfaces*, **2015**, 7, 24023–24031.
33. C. Yu, H. Gao, Q. Li and X. Cao, *Polym. Chem.*, 2020, 11, 3169–3178.
34. M. Handorf, Y. Zhou, M. A. Halanski and W. J. Li, *Organogenesis*, **2015**, 11, 1–15.
35. M. Matsusaki and M. Akashi, *Biomacromolecules*, **2005**, 6, 3351–3356.

Chapter 3.

Preparation of Injectable Poly(γ-glutamic acid)/Chondroitin Sulfate Hydrogels with Mineralization Ability

3.1 Introduction

Bone defects caused by trauma, tumors, and deformities are prevalent and have been reported worldwide.[1] Although bone possesses an excellent inherent repair capacity, its ability to bridge considerable defects remains limited. Invasive surgical procedures, such as autografts and allografts, are often necessary.[2] These procedures involve the integration of implants onto the bone lesion to stimulate proper bone repair.[3] Hydrogels serve as a platform for implantation of cells and provide proper mechanical strength to the surrounding tissues.[4–6] These properties allow cells to adhere and undergo differentiation on their matrices, and the subsequent degradation of hydrogels provides space for tissue regeneration. Poly(γ-glutamic acid) (PGA) has garnered considerable attention because of its excellent biodegradability, biocompatibility, and nontoxicity attributes.[7] PGA is a polypeptide secreted by *Bacillus subtilis* var. natto.[8] The large number of carboxylic acid groups on the PGA side chains are readily functionalized to achieve specific functions. In addition, the final degradation product of PGA is glutamic acid, which is a component of collagen and can provide the sites for apatite nucleation during bone formation.[9] Therefore, PGA has been employed to prepare hydrogels with diverse functions for applications in tissue engineering scaffolds, especially in cartilage and bone tissues.[10–13]

Spontaneous biomineralization is also an indispensable property for hydrogels used in bone tissue engineering.[14–16] Previous studies reported that PGA-based hydrogels exhibited excellent apatite-forming ability in simulated body fluid (SBF), since abundant carboxylic acid groups of PGA are effective for heterogeneous apatite nucleation.[17–21] For instance, Ohtsuki and Miyazaki et al. studied biomineralization behaviors of PGA-based hydrogels prepared by covalent crosslinking based on N-hydroxysuccinimide and 1-ethyl-3-(3-dimethylaminopropyl)-carbodiimide. Upon soaking in simulated body fluid (SBF), apatite

was observed on the surface of PGA-based hydrogels, which displayed fast apatite-forming rate in SBF via immersion or precursor solution mixture of calcium chloride ($CaCl_2$) solution.[17,19,21] Recently, polysaccharides containing sulfate groups were found to have the ability to induce apatite-forming, since abundant sulfate groups can tightly bind to calcium ions (Ca^{2+}), resulting in the enhancement of apatite nucleation.[22–24] Chondroitin sulfate (CS) is an anionic linear glycosaminoglycan composed of sulfated disaccharide repeating units with 1-3 linkages of D-glucuronic acid and N-acetylgalactosamine.[25,26] CS possesses anti-inflammatory activity and ability to enhance regeneration ability of bone defect or injury.[27] Because of the negative charge derived from sulfate groups, CS can establish an osteogenically favorable microenvironment via binding of charged ions, such as calcium and phosphate.[24] Currently, the main obstacle in the development of hydrogels for bone repair has been the difficulty in simultaneously achieving satisfactory injectability, mechanical properties and excellent apatite-forming ability, which has hindered the practical application of hydrogels.

Based on above considerations, in this study, inspired by the natural biomineralization feature of PGA and CS, versatile hydrogels based on hydrazide-modified PGA (PGA-ADH), oxidized chondroitin sulfate (OCS), and $CaCl_2$ were designed and synthesized via combination of dynamic acylhydrazone bonds and ionic bonding of acidic groups on polymer chains (carboxylic acid group (-COOH) or sulfate groups ($-OSO_3H$)) with Ca^{2+} ions. The dynamic acylhydrazone bonds imparted the hydrogels with injectability and self-healing properties. To the best of our knowledge, the influence of Ca^{2+} concentration on hydrogel performance, including gelation time, mechanical properties, self-healing ability, and apatite-forming behavior, has been comprehensively explored for the first time in the present study. The mechanical properties were tested using a rheometer. The structure and morphologies of mineralized hydrogels were characterized using powder X-ray diffraction (XRD) and scanning electron microscopy (SEM). Inductively coupled plasma atomic emission spectrometry (ICP-AES) was used to detect the atomic content of calcium and phosphorous in the mineralized hydrogels after immersion. The approximate apatite content of the mineralized hydrogels was estimated by conducting thermogravimetric analysis (TGA).

3.2 Experimental

Materials

Poly(γ-glutamic acid) (PGA, $M_w = 2.0 \times 10^6$ g/mol) (Seoul, Korea). Chondroitin sulfate (CS) and sodium periodate ($NaIO_4$) were purchased from Wako Chemicals (Osaka, Japan). 1-(3-Dimethylaminopropyl)-3-ethylcarbodiimide hydrochloride (EDC), N-hydroxysuccinimide (NHS), adipic dihydrazide (ADH) and 4-amino-L-phenylalanine monohydrate (4-amino-Phe) were obtained from Tokyo Chemical Industry (Tokyo, Japan). 2-Morpholinoethanesulfonic acid (MES) was purchased from Sigma-Aldrich (St. Louis, MO, USA). All reagents were used without further purification. For the preparation of SBF, reagent grade chemicals were purchased from Wako Chemicals and were used as received. The composition of SBF included NaCl (16.07 g), $NaHCO_3$ (0.71 g), KCl (0.45 g), $K_2HPO_4 \cdot 3H_2O$ (0.46 g), $MgCl_2 \cdot 6H_2O$ (0.62 g), $CaCl_2 \cdot 2H_2O$ (0.76 g), and tris(hydroxymethyl) aminomethane (12.24 g) in 1 L of deionized water.[28] The pH was adjusted to 7.4 at 37 °C.

Synthesis of OCS

CS (1.0 g, 2.1 mmol) was completely dissolved in 80 mL of deionized water at room temperature. $NaIO_4$ (0.7 g, 3.3 mmol) was added to the solution, and the reaction was subjected to oxidize in darkness for 3 h at 25 °C. Ethylene glycol (0.2 g, 3.3 mmol) was added with stirring for 30 min to stop this reaction. The solution was subjected to dialysis with deionized water for 3 days using a dialysis membrane with a molecular weight cut-off (MWCO) of 1×10^3. Thereafter, a white spongy OCS product was obtained by lyophilization (**Scheme 3-1**).

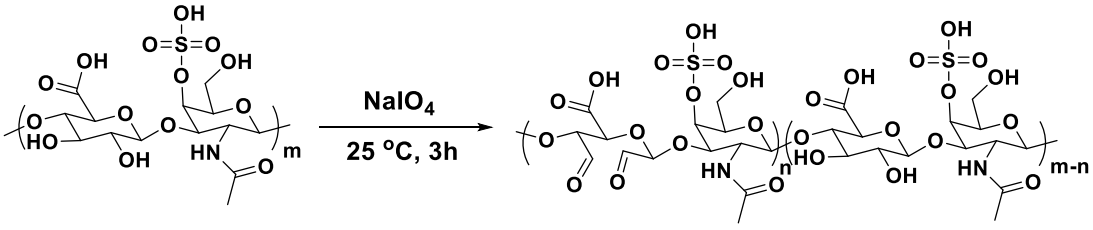

Scheme 3-1. Synthesis of OCS.

Synthesis of PGA-ADH

PGA (1.3 g, 10 mmol) was dissolved in 130 mL of MES buffer (0.1 mol/L, pH 5.5), Subsequently, the carboxylic groups were activated by adding EDC (2.3 g, 12 mmol), and NHS (1.2 g, 12 mmol) for 30 min. Then, ADH (2.6 g, 15 mmol) was added to this solution, and stirring of the mixture was conducted for 24 h at 25 °C. The reaction solution was subjected to dialysis against 0.1 mol/L NaCl solution for 3 days then deionized water for 3 days using a dialysis membrane with a MWCO of 1×10^4. Thereafter, a white spongy PGA-ADH product was obtained by lyophilization (**Scheme 3-2**).

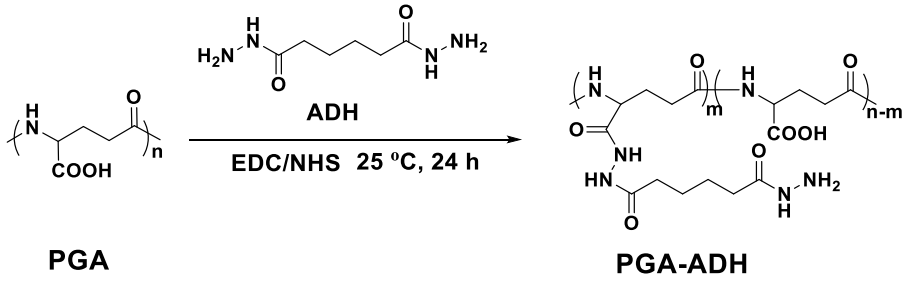

Scheme 3-2. Synthesis of PGA-ADH.

Preparation of hydrogels

The vial inversion method was used to determine the gelation time of the hydrogels. The synthetic route adopted for the hydrogels has been shown in **Scheme 3-3**. PGA-ADH (0.066 g) was dissolved in deionized water. Different volumes of 1.0 mol/L of $CaCl_2$ solution (0, 50, 200, 350, and 500 μL) were added to this solution to prepare solution A. Then OCS (0.060 g) and 4-amino-Phe (1.26 mg) were also dissolved in deionized water to prepare solution B. Here, 4-amino-Phe was used as a catalyst to accelerate the exchange of acylhydrazone bonds under mild conditions.[29] The pH values of solutions A and B were adjusted to 7.0 by adding 0.5 mol/L of NaOH solution. After a homogeneous solution was obtained, solution B was added to solution A and subjected to mixing, hydrogels were formed at room temperature. The total polymer concentration was maintained at 12.6% (w/v). The molar ratio of -$NHNH_2$ to -CHO was kept at 1:1. Based on the final concentration of the $CaCl_2$ solutions used herein (0, 0.05, 0.20, 0.35, and 0.50 mol/L), the resulting hydrogels were designated PCS, PCS-Ca-0.05, PCS-Ca-0.2,

PCS-Ca-0.35, and PCS-Ca-0.5, respectively. The formulation of hydrogels was listed in **Table 3-1**. To investigate the injectability of the hydrogels, rhodamine B was mixed with the prepared precursors of the hydrogels and drawn into a 20-gauge double syringe.

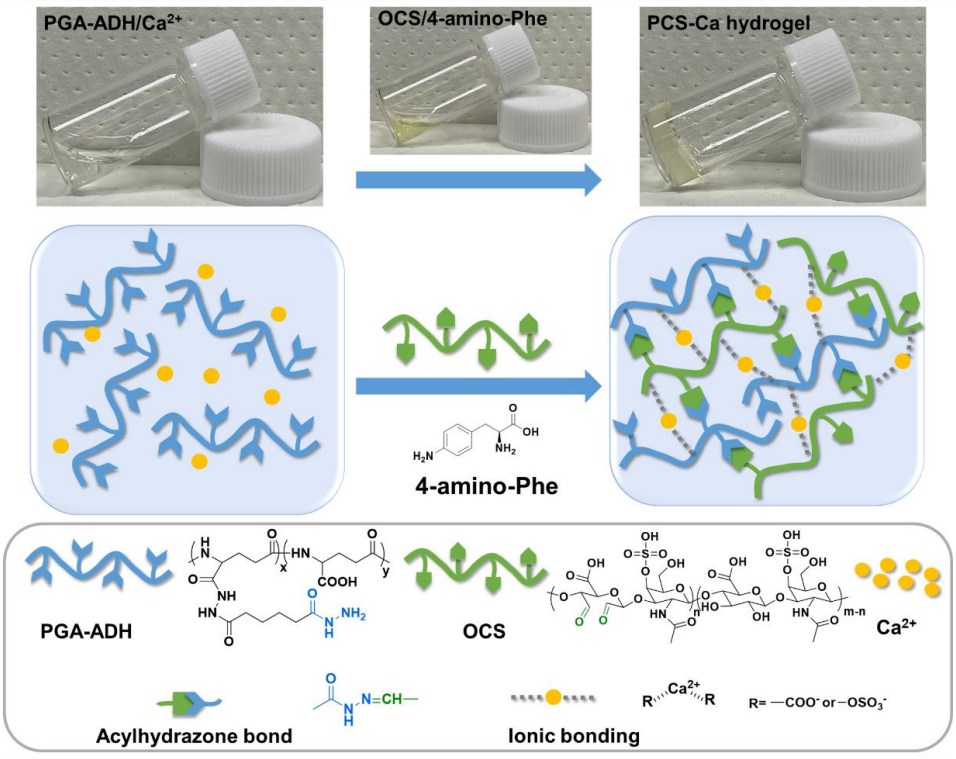

Scheme 3-3. Schematic representation of hydrogel formation

Table 3-1. Formulation of hydrogels.

Sample	-NHNH$_2$/-CHO [mol/mol]	$C_{Ca^{2+}}$ [mol/L][a]	$C_{polymer}$ [wt%][b]
PCS	1:1	0	12.6
PCS-Ca-0.05	1:1	0.05	12.6
PCS-Ca-0.2	1:1	0.2	12.6
PCS-Ca-0.35	1:1	0.35	12.6
PCS-Ca-0.5	1:1	0.5	12.6

[a] Ca^{2+} concentration in precursor solutions of hydrogels;

[b] Concentration of PGA-ADH and OCS in hydrogels.

Mechanical properties of hydrogels

Rheological analyses of the hydrogels were performed using the Hakke Rheostress 6000 (Thermo Fisher Scientific, Waltham, MA, USA) equipped with 20-mm diameter parallel plates. Hydrogels were placed at the bottom of the parallel plates. The oscillation frequency sweep was conducted using a range from 0.1 to 1.0 Hz at 0.1% strain under 37 °C to determine the modulus values of the hydrogels. To investigate the mechanical strength of the hydrogels, an axial ramp test was performed to obtain the compression stress-strain curve. The prepared cylindrical hydrogels (diameter: 13.0 mm; height: 5.0 mm) were loaded onto the bottom plate at a rate of 0.5 mm/s at 25 °C.

Self-healing ability test of hydrogels

Two hydrogel disks (diameter: 13.0 mm; height: 5.0 mm) were stained rhodamine B and methylene blue were cut in half using a 30 º wedged-shaped cutter. Subsequently, the two different colored semicircles were put together in the original mold and stored for 10 h at 37 ºC.

Immersion-mediated mineralization of hydrogels

The apatite-forming ability of the hydrogels was investigated by immersing the hydrogels in a 2×SBF solution. The cylindrical hydrogels were soaked in 10 mL of SBF solution and incubation was performed in a bio-shaker at 37 °C for 4 and 8 days, respectively, with exchange of fresh SBF solution every 24 h. After incubation, the mineralized hydrogels were rinsed with deionized water several times and were dried by lyophilization for further characterization.

Bio-adhesion of hydrogels

To investigate the integration of hydrogels with host bone, native bone harvested from the knee of an edible chicken was used to construct a hole host bone explant. The precursor solutions of the hydrogels were injected into the hole of the explant. Non-oxidized CS solution was mixed with PGA-ADH and $CaCl_2$ solution to fabricate an extremely weak hydrogel for establishing the control group. Push out test was performed to evaluate the adhesive strength of hydrogels with native bone.

Characterization

A lyophilized PGA-ADH sample was characterized by ^{1}H-NMR using the AVANCE 400 MHz apparatus (Bruker, Bremen, Germany) with D_2O as the solvent. Attenuated total reflection Fourier transform infrared (ATR-FTIR) spectroscopy was performed using the Nicolet iS5 apparatus (Thermo Fisher Scientific) to confirm the presence of -CHO after CS was subjected to oxidation. Powder XRD patterns of the hydrogels after mineralization were obtained using SmartLab (Rigaku Corporation, Tokyo, Japan) with a Cu K-beta X-ray source and a scanning speed of 2 ^{o} min^{-1} over a 2θ range of 5-55 ^{o}. The generator voltage and current were 45 kV and 200 mA, respectively. The morphologies of the hydrogels before and after mineralization were characterized by SEM using the SU3500 device (Hitachi). The hydrogel samples were freeze-dried and sputtered with gold using the MSP-1S magnetron sputter (Vacuum Device Inc., Osaka, Japan). The samples were observed under high vacuum conditions at an accelerating voltage of 1.50 kV. To investigate the generation rate of apatite in the mineralized hydrogels after immersion, the atomic content of phosphorous in the mineralized hydrogels was detected by inductively coupled plasma atomic emission spectrometry (ICP-AES) using the ICPS-8100 device (Shimadzu). Calcium and phosphorous standards were used for calibration. TGA was performed using the STA7200RV device (Hitachi) to evaluate the apatite content of the mineralized hydrogels in the temperature range of 40-700 ^{o}C at a heating rate of 10 ^{o}C min^{-1} under nitrogen protection conditions.

3.3 Results and discussion

Characterization of OCS and PGA-ADH

OCS with aldehyde groups was prepared via periodate oxidation of CS. As shown in **Figure 3-1**, the new peak at 1730 cm^{-1} was attributed to the aldehyde groups. Hydroxylamine hydrochloride titration for aldehyde groups revealed a 40.0% degree of oxidization.[30,31] PGA-ADH was synthesized via the EDC/NHS route. Representative ^{1}H NMR spectra of PGA, ADH, and PGA-ADH are presented in **Figure 3-2**. The alphabetically labeled peaks were assigned to the corresponding protons. The modification of PGA with ADH was confirmed by the presence

of the new peaks at 1.46 ppm corresponding to the methylene protons (4H, -CH_2CH_2-) of ADH. The resonance peak at 4.01 ppm was attributed to the binding of protons to the α-carbon of glutamic acid (1H, α-CH-) after completion of the reaction. The degree of substitution of PGA-ADH was 25.5%, as calculated by comparing the integral areas at 1.46 and 4.01 ppm.

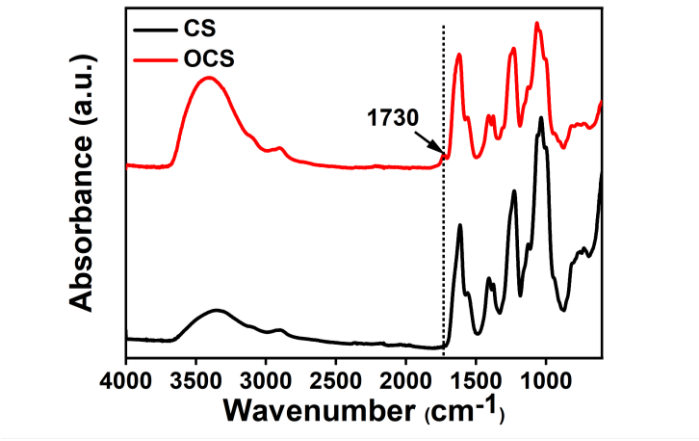

Figure 3-1. FTIR spectra of CS and OCS.

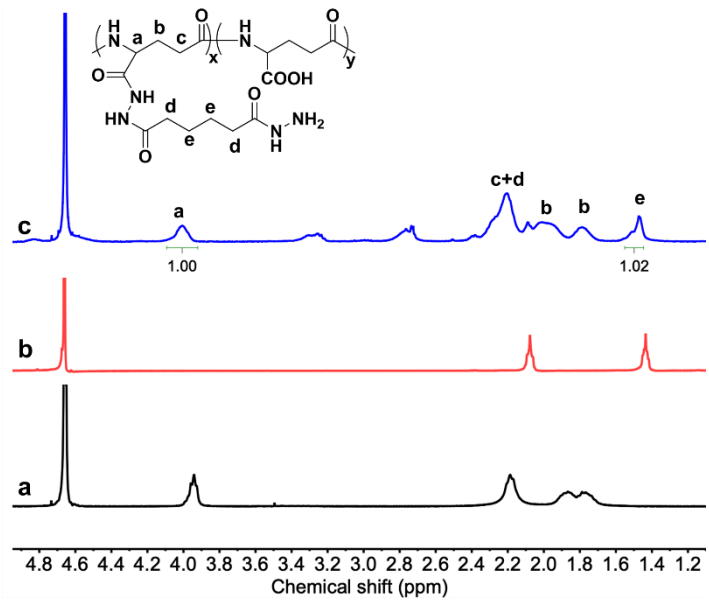

Figure 3-2. [1]HNMR spectra of (a) PGA, (b) ADH, and (c) PGA-ADH in D_2O.

Gelation time and injectability of hydrogels

Based on combination of acylhydrazone bonds and ionic bonding of acidic groups (-COOH

or -OSO_3H) on polymer chains with Ca^{2+} ions, hydrogels were prepared by mixing PGA-ADH and OCS in the presence of $CaCl_2$. An appropriate gelation rate is necessary for the practical application of injectable hydrogels. **Figure 3-3a** shows the gelation times of the hydrogels with and without the addition of $CaCl_2$. The gelation time of the PCS hydrogel was approximately 42 s. With increasing Ca^{2+} concentrations ranging from 0.05 to 0.35 mol/L, the gelation time of the PCS-Ca hydrogels changed from 44 s to 50 s, which was slightly longer than that observed with the PCS hydrogel. It is essential that injectable hydrogels used in bioengineering can be injected into irregular sites to enable the formation of a gel *in situ* to achieve the structural and functional restoration of damaged tissues. Owing to the rapid gelation based on the formation of acylhydrazone bonds, the extruded polymer solutions underwent assembly enable the formation of an integral hydrogel. Here, PCS-Ca-0.35 hydrogel precursors stained by rhodamine B injected into a Petri dish using a 20-gauge double syringe could present with the formation of different shapes. The letters "A" and "B" were successfully written, as shown in **Figure 3-3b**.

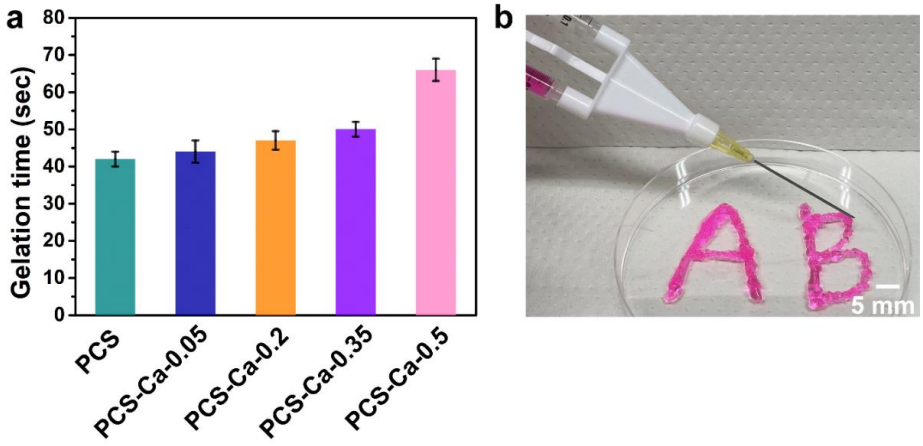

Figure 3-3. (a) Dependence of gelation time on the concentration of $CaCl_2$. (b) Photograph of the injectability of PCS-Ca-0.35.

Mechanical properties of hydrogels

To analyze the influence of Ca^{2+} concentration on the mechanical properties of the hydrogels, the modulus (*G'*/*G"*) of the hydrogels was measured by performing rheometer under a frequency sweep. The *G'* data at a fixed frequency of 1 Hz have been summarized in **Figure 3-**

4a. The *G'* of the PCS hydrogel was approximately 2100 Pa. The *G'* of the PCS-Ca hydrogels, except for the PCS-Ca-0.5 hydrogel, was evidently higher than that of the PCS hydrogel. When the Ca^{2+} concentration was in the range of 0.05 to 0.35 mol/L, the *G'* of the PCS-Ca hydrogels markedly increased and reached a maximum value of approximately 4200 Pa. This was associated with the ionic bonding established between the acidic group of the polymer chains and Ca^{2+} ions, leading to an increase in the crosslinking density. However, the *G'* of the PCS-Ca-0.5 hydrogel decreased when the Ca^{2+} concentration exceeded 0.35 mol/L, and this *G'* value was lower than that of PCS hydrogel. Based on these results, it was conceivable that excessive Ca^{2+} ions detrimentally influenced the formation and the performance of the PCS-Ca hydrogel. This was because the formation of coordination interaction of the Ca^{2+} ions and the hydrazide groups of PGA-ADH, the hydrazide groups were temporarily occupied, leading to a prolonged gelation time and the *G'* value of the hydrogel when the Ca^{2+} concentration was 0.5 mol/L. The compressive properties of hydrogels with different Ca^{2+} concentrations were evaluated as shown in **Figure 3-4b**. When the Ca^{2+} concentration increased to 0.35 mol/L, the compressive strength of the hydrogel was remarkably enhanced to 346.8 kPa, which is higher than that of other PGA-based hydrogels applied in cartilage or bone tissues.[32-34] Compared with the PCS hydrogel, the compressive strength and strain of the PCS-Ca-0.35 hydrogel improved 2.2 and 1.1 times, respectively. In contrast, the PCS-Ca-0.5 hydrogel displayed reduced compressive strength and strain. These phenomena could reflect a proper concentration range of Ca^{2+} ions (Ca^{2+} concentration range: 0.05-0.35 mol/L) that contributed to ionic bonding, thus increasing the crosslinking density of hydrogels and improving the compressive strength and strain. Of note, these results were the same as those observed for the gelation time and storage modulus described previously, suggesting that the presence of excessive Ca^{2+} ions could be detrimental to ionic bonding, resulting in a decrease in the mechanical properties of the hydrogels. Consequently, at moderate concentrations, Ca^{2+} ions improve the mechanical properties of the hydrogels. The subsequent experiments with PCS-Ca hydrogels were conducted using Ca^{2+} concentrations in the range of 0.05-0.35 mol/L.

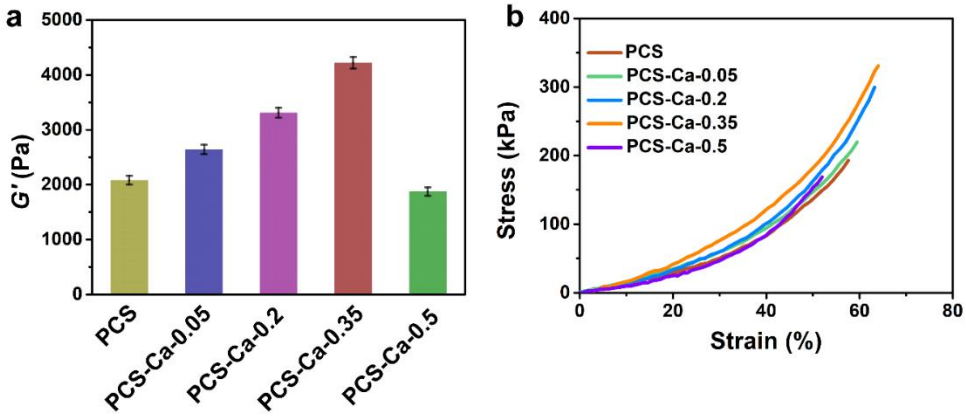

Figure 3-4. The *G'* (a) and compressive curves (b) of hydrogels.

Self-healing property of hydrogels

Self-healing of PCS-Ca hydrogels was evaluated by conducting direct visual examination. First, PCS-Ca-0.35 hydrogel disks were stained with rhodamine B and methylene blue (**Figure 3-5a**); the gels were then cut in half using a wedged-shaped cutter. The two different colored semicircles remained in close contact along the cut line (**Figure 3-5b**). The semicircles completely merged into an integral hydrogel disk after incubating at 37 ºC for 10 h without any external intervention (**Figure 3-5c**). The resulting hydrogel was adequately strong and withstood squeezing and tensile force without splitting (**Figure 3-5d,e**). This result demonstrated the excellent self-healing ability of the hydrogel.

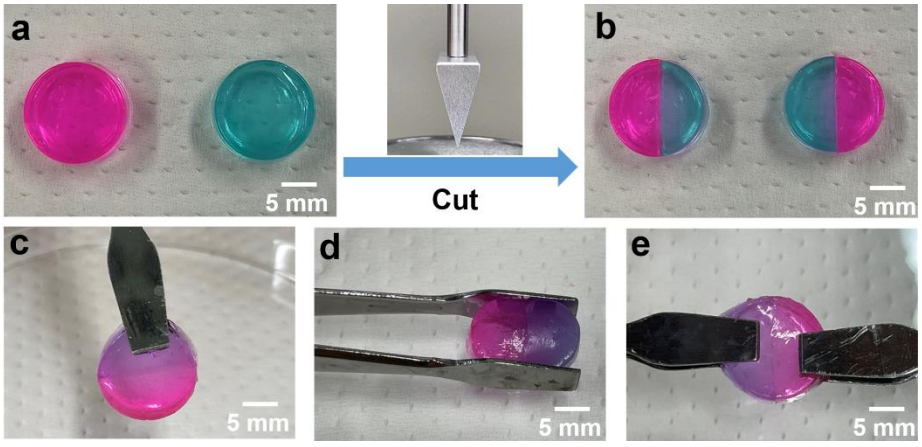

Figure 3-5. Photographs of the healing process of hydrogel. (a) Two hydrogel disks, (b) hydrogel disks were cut in half and placed together, (c-e) healing results of hydrogel after healing for 10 h at 37 °C.

Biomineralization of hydrogels

In vitro SBF incubation is a widely accepted method to examine the biomineralization process of scaffolds and to determine the applicability of the scaffold in bone tissue engineering. **Figure 3-6a** shows the XRD patterns obtained for the hydrogels after mineralization in 2× SBF for 4 days. By comparing with the database cart of hydroxyapatite (HAp) (reference code: 00-003-0747), XRD analysis of the mineralized hydrogels clearly demonstrated the presence of HAp phase with a crystal structure and main (002), (211), (222), (213), and (004) planes of HAp. The crystallinity index (CI) of mineralized hydrogels markedly increased from 9.8% to 22.4% with the addition of Ca^{2+} concentrations up to 0.35 mol/L (**Figure 3-6b**). Furthermore, after soaking for 8 days, mineralized hydrogels were analyzed by XRD; notably, the main XRD peaks displayed the same characteristics peak of the HAp phase; however, the CI of mineralized hydrogels soaked for 8 days presented an ascending trend (**Figure 3-6c,d**).

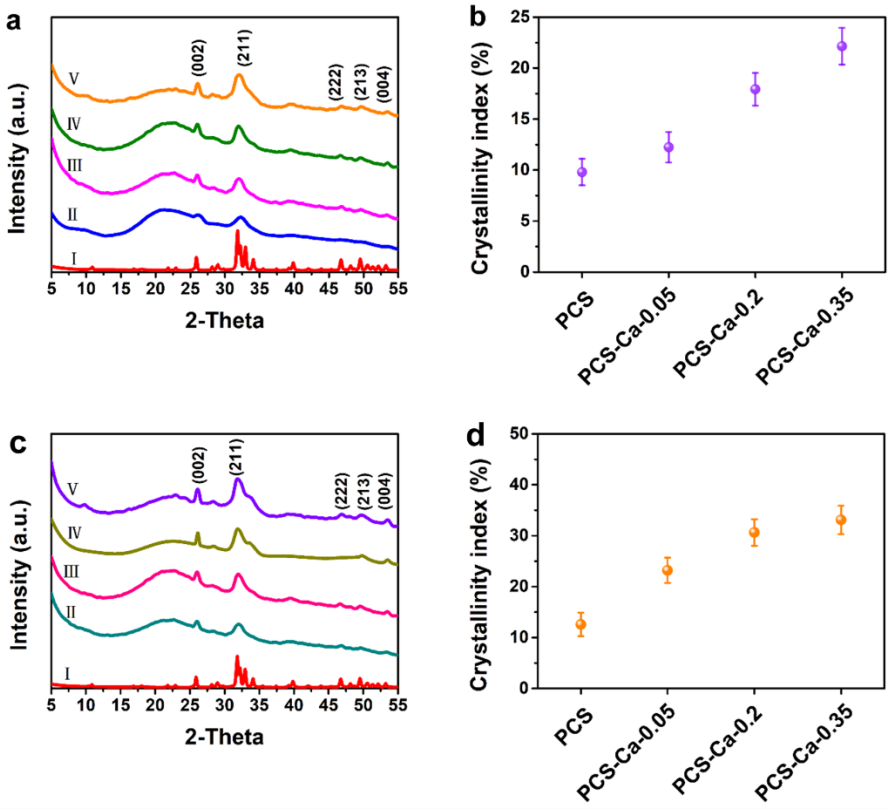

Figure 3-6. XRD and crystallinity index analyses. (a,c)XRD analysis of hydrogels after mineralization for 4 and 8 days. (b,d) Crystallinity index of hydrogels after mineralization for 4 and 8 days. ((Ⅰ) HAp, (Ⅱ) PCS, (Ⅲ) PCS-Ca-0.05, (Ⅳ) PCS-Ca-0.2, and (Ⅴ) PCS-Ca-0.35)

Morphologies of the surfaces of the mineralized hydrogels were characterized using SEM (**Figure 3-7**). An apatite precipitation layer was appeared on the surfaces of hydrogels after immersion for various periods. Compared **Figure 3-7a,e**, the surface of the PCS hydrogel was only partially precipitated with apatite layers in the early stage of immersion, but after 8 days of immersion, more apatite covered the hydrogel surface. It is noteworthy that visibly granular apatite was formed on the surfaces of hydrogels with the immersion time and the increase of Ca^{2+} concentration. Furthermore, morphologies of the cross-sections of hydrogels were explored as shown in **Figure 3-8.** Before mineralization, a smooth porous structure was observed (**Figure 3-8a-d**). After 4 days of immersion, apatite deposition was markedly observed in the pores of hydrogels (**Figure 3-8e-h**). The density of apatite deposition increased apparently when the immersion time was prolonged to 8 days (**Figure 3-8i-l**), indicating that the biomineralization of the interior of hydrogels was dependent on the immersion time. Compared with the PCS hydrogel, the apatite deposition was denser in the interior of the PCS-Ca hydrogels with increasing Ca^{2+} concentration. The findings suggested that the immersion time and the presence of Ca^{2+} ions were conducive to the induction of apatite formation in the interior of hydrogels. For the application of apatite-polymer porous materials as a scaffold for bone regeneration, the formation of a bioactive layer within the pore is preferable for the realization of healthy bone growth.

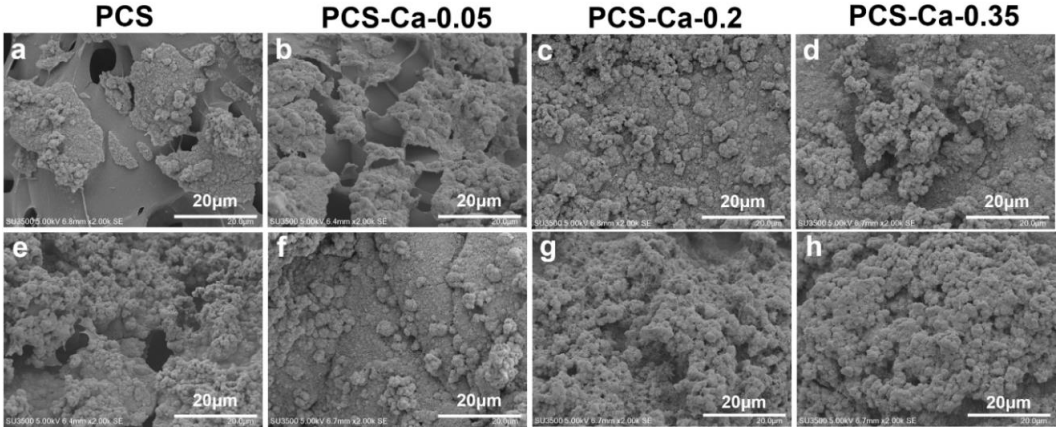

Figure 3-7. SEM images of the surfaces of hydrogels after mineralization for 4 (a-d) and 8 days (e-h).

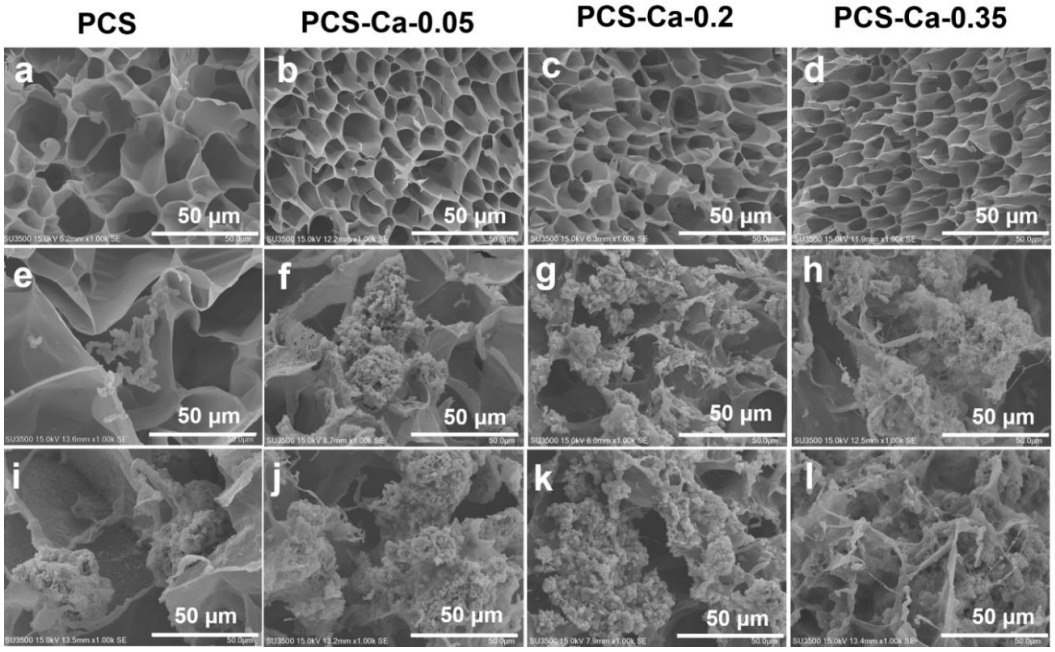

Figure 3-8. SEM images of the cross-sections of hydrogels before mineralization (a-d), after mineralization for 4 days (e-h) and 8 days (i-l).

To further investigate the influencing factors during apatite formation in hydrogels, ICP-AES was performed to estimate the calcium (Ca) and phosphorus (P) concentrations of apatite in mineralized hydrogels. As shown in **Figure 3-9a**, Ca concentration of PCS hydrogel increased with immersion time. In contrast, Ca concentration of PCS-Ca hydrogels first dropped in the 0.5 or 1 day, and then slowly increased with immersion time, indicating that a portion of Ca^{2+} ions in the hydrogels would diffuse into SBF. The released Ca^{2+} ion from PCS-Ca-0.35 hydrogel was larger than that from PCS-Ca hydrogels with lower Ca^{2+}. Compared with the SEM results of the surfaces of mineralized hydrogels, it was sepeculated that apatite deposition layers are noticeably accelerated by Ca^{2+} release from the hydrogels into the SBF, which locally increases the degree of supersaturation of the surrounding fluid with respect to apatite. In addition, the un-released Ca^{2+} ions in the hydrogels lead to their internal mineralization, because SBF penetrated inside the hydrogels contributes to form apatite deposition in the pores of hydrogels when Ca^{2+} ions remain in the hydrogels. This could explain SEM results of the cross-sections of mineralized hydrogels. The P concentration of hydrogels increased remarkably in early stages of immersion with increasing Ca^{2+} concentration, and was relatively constant after 6 days

of soaking, as displayed in **Figure 3-9b**. Therefore, it could be inferred in that the apatite content in the PCS-Ca hydrogels was higher than that in the PCS hydrogel, especially in early periods of immersion, demonstrating that the presence of Ca^{2+} ions mainly accelerated the mineralization rate of hydrogels in the early period.

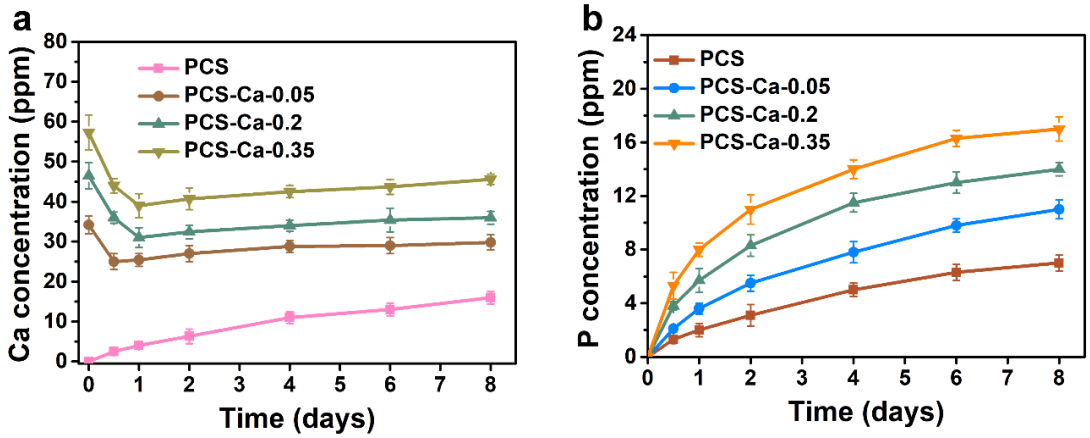

Figure 3-9. Dependence of calcium (a) and phosphorus (b) concentrations of mineralized hydrogels on immersing time.

Additionally, TGA was performed to determine the total amount of apatite in the hydrogels after immersion in SBF for 8 days (**Figure 3-10**). The amount of apatite in mineralized hydrogels with different Ca^{2+} concentrations (0, 0.05, 0.2, and 0.35 mol/L) was 6.9%, 9.7%, 11.5%, and 18.2%, respectively. Compared with the cellulose-based mineralized hydrogel (around 2 weeks),[35,36] PGA-based hydrogel took short period (around 1 week) to form an equal amount of apatite in the same immersion conditions in this work. This indicated the hydrogels composed of PGA and CS exhibited a rapid mineralization rate. Mineralized hydrogels with increasing levels of Ca^{2+} ions presented with higher apatite content, a finding that was identical to the finding noted in terms of the morphology and ICP-AES analysis results. Overall, these results demonstrate that PCS-Ca hydrogels are a novel and robust template for the rapid *in situ* mineralization of apatite. The existence of Ca^{2+} ions in hydrogels was conducive to increase the degree of apatite supersaturation,[26] thus allowing rapid rate of apatite formation and high apatite content in hydrogels after soaking in SBF.

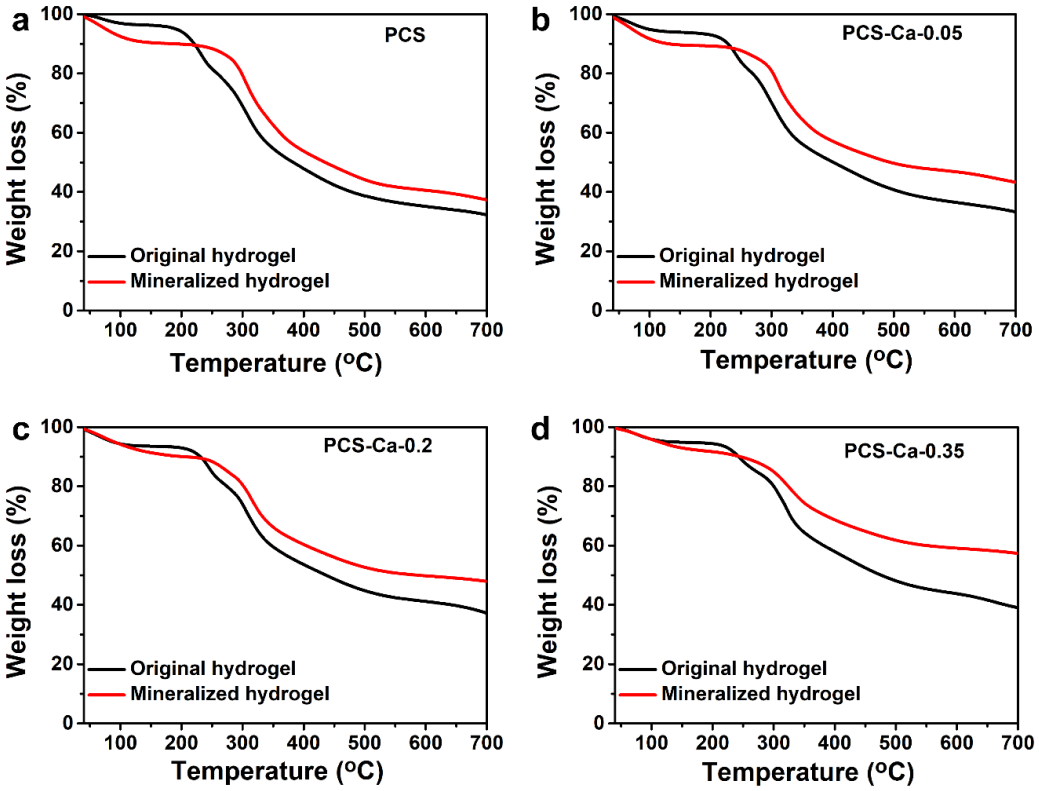

Figure 3-10. TGA curves of the unmineralized and mineralized hydrogels. (a) PCS, (b) PCS-Ca-0.05, (c) PCS-Ca-0.2, (d) PCS-Ca-0.35

Bio-adhesion of hydrogels

The bio-adhesive properties of hydrogels were investigated using chicken bone. CS that was not oxidized was mixed with PGA-ADH and Ca^{2+} ion solution to form a weak hydrogel as the control group. As displayed in **Figure 3-11a,b**, when the hydrogels were lifted with the tweezer, the control hydrogel could not adhere with the local bone tissue, while PCS-Ca-0.35 hydrogel exhibited good bio-adhesion to the bone. This was because the presence of aldehyde groups in hydrogels aids Schiff base reaction between aldehydes and amines of local bone tissue.[37,38] The adhesive strength of hydrogels with chicken bone tissue was evaluated by push-out test as shown in **Figure 3-11c**. The adhesive strength of PCS-Ca-0.35 hydrogel and bone was 26.4 kPa, which was obviously higher than that of control hydrogel (2.2 kPa). The findings demonstrated that the aldehyde-amine Schiff base reaction allowed the bio-adhesion of the hydrogel and native bone tissues. The prepared hydrogels exhibited good tissue-adhesive properties, and such properties could be considered for potential application in bone tissue engineering scaffolds.

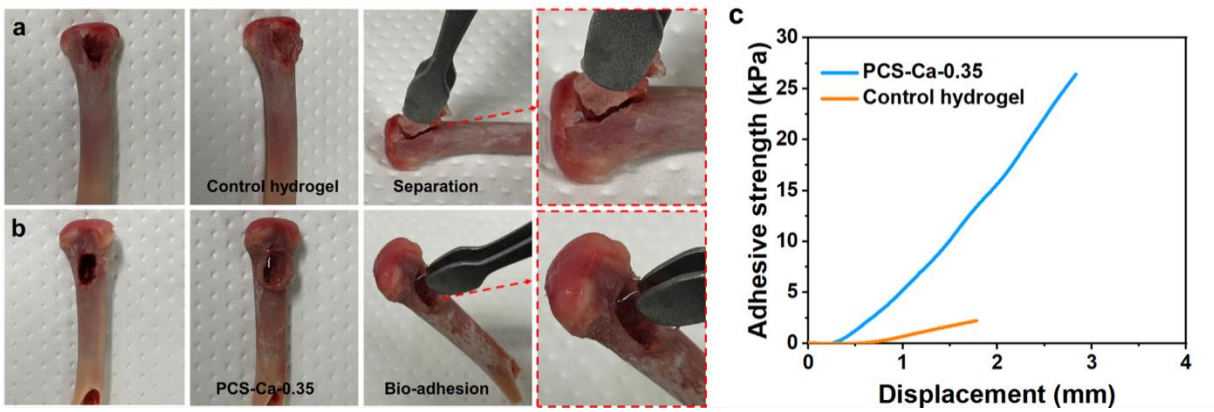

Figure 3-11. Photographs of bio-adhesion of hydrogels and chicken bone. (a) control hydrogel, (b) PCS-Ca-0.35. (c) Adhesive strength curve of hydrogels and chicken bone.

3.4 Conclusions

A series of self-healing and injectable hydrogels were prepared successfully using hydrazide-modified PGA and oxidized CS through the formation of dynamic acylhydrazone bonds and ionic bonding of acidic groups of polymer chains with Ca^{2+} ions. The hydrogels exhibited rapid gelation within 50 s. Compared with hydrogels without Ca^{2+} ions, the mechanical properties of the hydrogels prepared using appropriate concentrations of Ca^{2+} ions were remarkably enhanced, implying that the Ca^{2+} ionic bonding exerted an outstanding effect on hydrogels performance. The hydrogels exhibited self-healing ability under physiological conditions. Moreover, apatite-forming ability of the hydrogels was promoted in the presence of Ca^{2+} ions after immersion in SBF. These results indicated that addition of Ca^{2+} ions to the hydrogels enhanced mechanical strength, and facilitated rapid mineralization. Furthermore, hydrogels displayed good tissue-adhesive properties due to the occurrence of the aldehyde-amine Schiff base reaction. The collective findings demonstrate the promising potential utility of these injectable and self-healing hydrogels with rapid apatite formation in bone regeneration.

References

1. W. Wang and K. W. K. Yeung, *Bioact. Mater.*, **2017**, 2, 224–247.
2. A. R. Amini, C. T. Laurencin and S. P. Nukavarapu, *Crit. Rev. Biomed. Eng.* **2012**, 40 (5), 363−408.
3. A. N. Ball, S. W. Donahue, S. J. Wojda, C. W. McIlwraith, C. E. Kawcak, N. Ehrhart and L. R. Goodrich, *J. Orthop. Res.*, **2018**, 36, 1559–1572.
4. P. Abdollahiyan, F. Oroojalian, A. Mokhtarzadeh and M. de la Guardia, *Biotechnol. J.*, **2020**, 15, 2000095.
5. K. Lei, Z. Li, D. Zhu, C. Sun, Y. Sun, C. Yang, Z. Zheng and X. Wang, *J. Mater. Chem. B*, **2020**, 8, 794–802.
6. K. Lei, K. Wang, Y. Sun, Z. Zheng and X. Wang, *Adv. Funct. Mater.*, **2021**, 31, 1–11.
7. S. Bin Park, M. H. Sung, H. Uyama and D. K. Han, *Prog. Polym. Sci.*, **2021**, 113, 101341.
8. T. Tanaka, K.-I. Fujita, S. Takenishi and M. Taniguchi, *J. Ferment. Bioeng.*, **1997**, 84, 361–364.
9. C. Gao, S. Ito, A. Obata, T. Mizuno, J. R. Jones and T. Kasuga, *Polymer*, **2016**, 91, 106–117.
10. R. Yang, X. Wang, S. Liu, W. Zhang, P. Wang, X. Liu, Y. Ren, X. Tan and B. Chi, *Int. J. Biol. Macromol.*, **2020**, 142, 332–344.
11. S. Liu, Y. Pu, R. Yang, X. Liu, P. Wang, X. Wang, Y. Ren, X. Tan, Z. Ye and B. Chi, *Int. J. Biol. Macromol.*, **2020**, 153, 158–168.
12. X. Ma, X. Liu, P. Wang, X. Wang, R. Yang, S. Liu, Z. Ye and B. Chi, *ACS Appl. Bio Mater.*, **2020**, 3, 4036–4043.
13. P. Wang, W. Zhang, R. Yang, S. Liu, Y. Ren, X. Liu, X. Tan and B. Chi, *Int. J. Biol. Macromol.*, **2021**, 167, 1508–1516.
14. B. Xu, P. Zheng, F. Gao, W. Wang, H. Zhang, X. Zhang, X. Feng and W. Liu, *Adv. Funct. Mater.*, **2017**, 27, 1604327.
15. L. C. Palmer, C. J. Newcomb, S. R. Kaltz, E. D. Spoerke and S. I. Stupp, *Chem. Rev.*, **2008**, 108, 4754–4783.
16. X. Xue, Y. Hu, Y. Deng and J. Su, *Adv. Funct. Mater.*, **2021**, 31, 2009432.
17. A. Sugino, T. Miyazaki and C. Ohtsuki, *Key Eng. Mater.*, **2007**, 330–332, 683–686.
18. M. Y. Koh, C. Ohtsuki and T. Miyazaki, *J. Biomater. Appl.*, **2011**, 25, 581–594.
19. T. Miyazaki, J. Mukai, E. Ishida and C. Ohtsuki, *Biomed. Mater. Eng.*, **2013**, 23, 339–347.
20. T. Miyazaki, A. Kuramoto, A. Hirakawa, Y. Shirosaki and C. Ohtsuki, *Dent. Mater. J.*, **2013**, 32, 544–549.
21. A. Sugino, T. Miyazaki and C. Ohtsuki, *J. Mater. Sci. Mater. Med.*, **2008**, 19, 2269–2274.
22. I. Y. Kim, R. Iwatsuki, K. Kikuta, Y. Morita, T. Miyazaki and C. Ohtsuki, *Mater. Sci. Eng. C*, **2011**, 31, 1472–1476.
23. R. Nakata, T. Miyazaki, Y. Morita, E. Ishida, R. Iwatsuki and C. Ohtsuki, *J. Ceram. Soc. Japan*, **2010**, 118, 487–490.

24. H. D. Kim, E. A. Lee, Y.-H. An, S. L. Kim, S. S. Lee, S. J. Yu, H. L. Jang, K. T. Nam, S. G. Im and N. S. Hwang, *ACS Appl. Mater. Interfaces*, **2017**, 9, 21639–21650.
25. R. A. A. Muzzarelli, F. Greco, A. Busilacchi, V. Sollazzo and A. Gigante, *Carbohydr. Polym.*, **2012**, 89, 723–739.
26. Y. Shi, Y. Meng, J. Li, J. Chen, Y. Liu and X. Bai, *J. Chem. Technol. Biotechnol.*, **2014**, 89, 1445–1465.
27. B. N. Singh, V. Veeresh, S. P. Mallick, S. Sinha, A. Rastogi and P. Srivastava, *Int. J. Biol. Macromol.*, **2020**, 153, 1–16.
28. T. Kokubo and H. Takadama, *Biomaterials*, **2006**, 27, 2907–2915.
29. X. Yang, G. Liu, L. Peng, J. Guo, L. Tao, J. Yuan, C. Chang, Y. Wei and L. Zhang, *Adv. Funct. Mater.*, **2017**, 27, 1–10.
30. J. Thomas, A. Sharma, V. Panwar, V. Chopra and D. Ghosh, *ACS Appl. Bio Mater.*, **2019**, 2, 2013–2027.
31. D. A. Wang, S. Varghese, B. Sharma, I. Strehin, S. Fermanian, J. Gorham, D. H. Fairbrother, B. Cascio and J. H. Elisseeff, *Nat. Mater.*, **2007**, 6, 385–392.
32. P. Wang, Y. Pu, Y. Ren, R. Yang, W. Zhang, X. Tan, W. Xue, S. Liu, S. Li and B. Chi, *Carbohydr. Polym.*, **2022**, 275, 118692.
33. D. Puppi, C. Migone, L. Grassi, A. Pirosa, G. Maisetta, G. Batoni and F. Chiellini, *Polym. Int.*, **2016**, 65, 631–640.
34. P. Wang, W. Zhang, R. Yang, S. Liu, Y. Ren, X. Liu, X. Tan and B. Chi, *Int. J. Biol. Macromol.*, **2021**, 167, 1508–1516.
35. A. Salama, R. E. Abou-Zeid, I. Cruz-Maya and V. Guarino, *Carbohydr. Polym.*, **2020**, 229, 115472.
36. R. E. Abouzeid, R. Khiari, D. Beneventi and A. Dufresne, *Biomacromolecules*, **2018**, 19, 4442–4452.
37. F. Yu, X. Cao, J. Du, G. Wang and X. Chen, *ACS Appl. Mater. Interfaces*, **2015**, 7, 24023–24031.
38. J. Xu, Y. Liu and S. Hsu, *Molecules*, **2019**, 24, 3005.

Concluding Remarks

In this work, responsive hydrogels using PGA backbone were developed. The PGA-based hydrogels displayed with pH and ionic responsiveness due to the inherent carboxylic acid groups of on the side chain of PGA. Moreover, the hydrogels possessed enzymatic and body temperature responsiveness because of the modification of carboxylic acid groups on the side chain of PGA.

In Chapter 1, pH-responsive hydrogels comprised of PGA modified with tyramine (PGA-Tyr) were developed through enzymatic cross-linking in the presence of HRP and H_2O_2. The gelation rate and stiffness of the resulting hydrogels were tuned by changing the concentrations of HRP and H_2O_2 or the degree of substitution (DS) of PGA-Tyr. The hydrogels exhibited a good reversibility of pH responsiveness in pH 2.0 and 7.0 solutions. The degradation rate of the hydrogels in simulated intestinal fluid (SIF) was faster than that in simulated gastric fluid (SGF). Moreover, indomethacin (IM), a hydrophobic drug model, was encapsulated in the hydrogels, and the pH-dependent drug release of IM-loaded hydrogels was achieved in SGF and SIF. Importantly, when IM was entrapped in pluronic F-127 to form drug micelles, the burst release of the IM-micelle-loaded hydrogels with a high DS of PGA-Tyr was remarkably decreased in SGF, and sustained drug release was presented in SIF. Thus, pH-responsive PGA-based hydrogels have tremendous promise for biomedical applications, especially oral drug delivery.

In Chapter 2, injectable PGA-based hydrogels were constructed using furfurylamine and tyramine-modified PGA (PGA-Fa-Tyr) and the crosslinker dimaleimide poly(ethylene glycol), through a facile strategy combining enzymatic cross-linking and Diels-Alder (DA) reaction. The hydrogels possessed rapid gelation time. The mechanical properties of hydrogels could be easily adjusted by changing the concentration of H_2O_2. Furthermore, the mechanical properties of the hydrogels were remarkably enhanced when temperature increased from 25 ^oC to 37 ^oC. This was because the DA reaction was occurred in the hydrogels under the stimulation of body temperature. The injectable hydrogels could be degraded in the PBS solution with proteinase K. The BSA-loaded hydrogels exhibited a sustained release behavior. Thus, the developed

hydrogels hold great potential for applications in biomedical fields, such as tissue engineering and cell/drug delivery.

In Chapter 3, injectable hydrogels were fabricated using hydrazide-modified PGA and oxidized chondroitin sulfate by combining acylhydrazone bonds and ionic bonding of carboxylic acid groups or sulfate groups with calcium ions (Ca^{2+}). The resulting hydrogels displayed a fast gelation rate and good self-healing ability. The hydrogels could response to Ca^{2+} ions. The introduction of Ca^{2+} at a moderate concentration enhanced the mechanical strength of the hydrogels. The mineralized hydrogels with increasing Ca^{2+} concentration exhibited rapid formation and high crystallization of apatite after immersion in simulated body fluid. The hydrogels containing the aldehyde groups possessed good bio-adhesion to the bone tissues. With these superior properties, the developed hydrogels demonstrate potential applicability in bone tissue engineering.

In summary, different strategies were designed to develop versatile hydrogels using PGA backbone. The responsive properties of hydrogels were endowed based on the inherent features of PGA and the introduction of responsive groups to PGA. The presented strategies for developing functional PGA-based hydrogels will contribute to developing the next generation of responsive polypeptide-based hydrogels. The author believes this work will open a door to an exploration of polypeptide-based hydrogels as novel biomaterials in practical biomedical applications.

List of Publications

1. Preparation of pH-Responsive Poly(γ-glutamic acid) Hydrogels by Enzymatic Cross-Linking

Meng Wei, Tomonori Inoue, Yu-I Hsu*, Moon-Hee Sung, Tokuma Fukuoka, Shiro Kobayashi, and Hiroshi Uyama*

ACS Biomaterials Science & Engineering, **2022**, *8(2)*: 551-559.

DOI: 10.1021/acsbiomaterials.1c01378

2. Injectable Poly(γ-glutamic acid)-based Biodegradable Hydrogels with Tunable Gelation Rate and Mechanical Strength

Meng Wei, Yu-I Hsu*, Taka-Aki Asoh, Moon-Hee Sung, and Hiroshi Uyama*

Journal of Materials Chemistry B, **2021**, *9(16)*: 3584-3594.

DOI: 10.1039/D1TB00412C

3. Design of Injectable Poly(γ-glutamic acid)/Chondroitin Sulfate Hydrogels with Mineralization Ability

Meng Wei, Yu-I Hsu*, Taka-Aki Asoh, Moon-Hee Sung, and Hiroshi Uyama*

ACS Applied Bio Materials, **2022**, *5(4)*: 1508–1518.

DOI: 10.1021/acsabm.1c01269

Acknowledgments

This study was carried out from 2019 to 2022 at Department of Applied Chemistry, Graduate School of Engineering, Osaka University. The doctoral dissertation is mainly studied with the preparation of versatile poly(γ-glutamic acid)-based hydrogel. This work could not be completed without the support and help of the people around me. Therefore, I deeply appreciate to all of them for their kind help over the three years.

First and foremost, I would like to appreciate Prof. Hiroshi Uyama, my supervisor, who provided me precious opportunities and constant support during my PhD and acted as a role model to me not only academically but also in life. He provided me a chance to study in Japan and continue studying the filed what I am interested. And the use of natto-derived poly(γ-glutamic acid) as raw material made me like eating natto. He also supported me to apply CSC scholarship. Over the past three years, he gave me a lot of instruction, research advice, encouragement and freedom for my research. Besides my advisor, I would like to thank the rest of my thesis committee: Prof. Satoshi Minakata and Prof. Norimitsu Tohnai, for their insightful comments and useful advice.

Additionally, I appreciate Prof. Yu-I Hsu, Associate Professor in our group. At the beginning of my research, I was not sure about the connection between materials and biomedical applications. Under her guidance, I gradually learned more about biomedical aspects, which led me to open the door of biomedical fields. I also would like to thank her patient revisions and advice for my papers, and her warm concern for my life.

I am profoundly grateful to Prof. Moon-Hee Sung for providing the poly(γ-glutamic acid) so that I can conduct my work. Many thanks to Prof. Taka-aki Asoh for teaching me how to think scientifically and logically, and he also gave me a lot of professional advice for my study.

I also appreciate Assistant Prof. Akihide Sugawara to revise the doctoral abstract, slides and etc. He helped me and gave useful strategies for my experimental. I will never forget the happy trip to Universal Studios Japan in 2019.

I wish to appreciate the kind help and warm-hearted support from Ms. Yoko Uenishi and Ms. Tomoko Shimizu.

I want to thank the lovely and kind members in Uyama Lab: Dr. Xinnan Cui, Dr. Masatoshi

Kato, Dr. Chen Qian, Dr. Zhengtian Xie, Dr. Yankun Jia, Dr. Toshiki Tamiya, Dr. Shunsuke Mizuno, Dr. Hanyu Wen, Dr. Yanting Lyu, Dr. Naharullah Bin Jamaluddin, Dr. Raghav Soni, Mr. Mark Adam Malaluan Ferry, Mr. Luwei Zhang, Ms. Yan Wang, Ms. Manjie He, Mr. Yuxiang Jia, Ms. Juan Wang, Mr. Peng Du, Ms. Zeying Cao, Ms. Linxuan Li, Ms. Xunran Guo, Ms. Alice, Ms. Guan Wang, Ms. Ying Yao, Mr. Toshiki Honda, Ms. Airi Ozaki, Mr. Yuya Fujiwara, Ms. Yuka Kashihara, Mr. Yuji Kiba, Mr. Takeshi Hiraoka, Mr. Atsushi Koizumi, Mr. Yuki Shioji, Mr. Nontarin Roopsung, Mr. Emil Hajili, Ms. Madhurangika Panchabashini Horathal Pedige, Ms. May Myat Noe, Ms. Hasinah Binti Mohamed Rafiq, Ms. Judit Rebeka Molnar, Ms. Izzah Durrati Binti Haji Abdul Hamid, Ms. Sooyeon Noh, Ms. Thuy Le Huynh An, Mr. Motoi Oda, Ms. Suzune Miki, Mr. Kaita Kikuchi, Mr. Koki Tsujita, Mr. Hajime Fujimori, Ms. Rika Onishi, Mr. Shotaro Yano, Ms. Rina Kugimiya, Ms. Kyoko Tanimura, Ms. Chikabo Abe, Ms. Erina Katsuragawa, Mr. Yasushi Takeuchi, and Mr. Atsuki Takagi, etc. for their kind-hearted help in my lab and daily life.

I also want to thank my friends: Ms. Meng Niu, Ms. Cong Gao, Dr. Miaomiao Wen, Dr. Bozhi Chen, Dr. Hanyu Wen, Ms. Yan Wang, Ms. Yingbu Liu, Dr. Haomin Yan. Thanks to them, true friendship made my research life full of energy and joy.

I am also grateful that the China Scholarship Council generously offered a scholarship to support my doctoral study in Japan.

Finally, I would like to thank all my family members: my grandparents, my parents, my uncle, my husband (Junyi Han), and his parents for endless supporting me spiritually in my research and daily life. I will always remember what my grandmother said to me when I was a child: be an independent girl with your own judgment, choose the way you like and be brave enough to pursue to it. I feel very lucky that I walked through the PhD way with the help from many people around me in the past three years, and I will continue to keep enthusiasm in the future. And special thanks to my husband for his love, his strict for my experimental and his support in life. These were most memorable three years I have had. While challenging, it was undoubtedly exciting. Thank you for everyone I have met along the way.

Suita, Osaka, Japan

June 2022

Meng Wei